iScience

Article

Growth of human regulatory CD4$^+$ T cells is more tightly controlled than effector T cells due to distinctive molecular programming

Graphical abstract

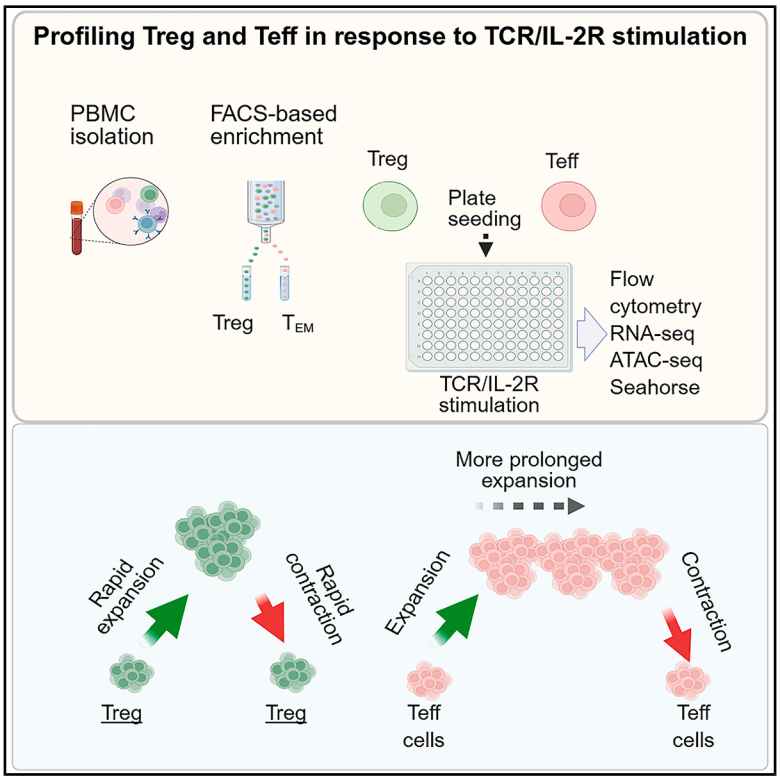

Highlights

- Tregs are programmed to more rapidly contract than Teff cells
- Tregs depend on frequent re-engaging the TCR pathway for continued expansion
- Transcriptomic and epigenomic changes in Teff cells favor more prolonged expansion
- Teff cells better activate mTORC1 and Myc pathways for a higher energetic phenotype

Authors

Alejandro Moro, Aixin Yu, Luis Nivelo, Zhen Gao, Yuguang Ban, Alejandro V. Villarino, Thomas R. Malek

Correspondence

tmalek@med.miami.edu

In brief

Immunology; Components of the immune system

Moro et al., 2025, iScience *28*, 112553
June 20, 2025
https://doi.org/10.1016/j.isci.2025.112553

CellPress

iScience

CellPress
OPEN ACCESS

Article

Growth of human regulatory CD4$^+$ T cells is more tightly controlled than effector T cells due to distinctive molecular programming

Alejandro Moro,[1] Aixin Yu,[1] Luis Nivelo,[1] Zhen Gao,[2] Yuguang Ban,[2,3] Alejandro V. Villarino,[1] and Thomas R. Malek[1,4,*]
[1]Department of Microbiology and Immunology, Miller School of Medicine, University of Miami, Miami, FL 33136, USA
[2]Sylvester Comprehensive Cancer Center, University of Miami, Miami, FL, USA
[3]Division of Biostatistics, Department of Public Health Sciences, University of Miami, Miami, FL, USA
[4]Lead contact
*Correspondence: tmalek@med.miami.edu
https://doi.org/10.1016/j.isci.2025.112553

SUMMARY

Foreign and self-antigens activate CD4$^+$ conventional and regulatory T cells (Tregs) to promote immunity and tolerance, respectively. These cell populations, which depend on interleukin-2 (IL-2), are being expanded and engineered *in vitro* for adoptive cell therapy (ACT) for cancer and autoimmunity. Here, we investigate the molecular pathways underlying the *in vitro* expansion of human CD4$^+$ Teff and Tregs to TCR/CD28/IL-2 signaling over 12-days. Temporal integration of differential chromatin accessibility and gene expression revealed similar responses over the first 6 days. After this time, T effector (Teff) cells showed greater expansion that was associated with more robust gene activation and chromatin opening that supported increased activation of mTORC1-dependent signaling and a more energetic phenotype. Thus, Tregs are programmed temporally for more limited expansion *in vitro* that may benefit ACT for cancer but may be a drawback for autoimmunity. These findings may reflect a mechanism to finely tune Treg numbers to maintain homeostasis *in vivo*.

INTRODUCTION

The interleukin-2 (IL-2)/IL-2R system is essential for regulation of tolerance and immunity. Signaling through the high affinity IL-2R (K_d 10^{-11} M), comprising CD25 (IL-2Rα), CD122 (IL-2Rβ), and CD132 (γc), is required for optimal clonal expansion of antigen-reactive T cells and their development and programming into highly functional T effector (Teff) and memory cells, respectively.[1] This signaling is also essential for thymic development of regulatory T cells (Tregs) and their survival in the periphery.[1–7] IL-2 also supports Treg proliferation.[8,9] The proliferative activity of IL-2 for Treg and Teff cells *in vitro* does not act alone but requires activation through the T cell receptor (TCR) and co-stimulation through CD28.[10,11] The requirement for TCR and co-stimulatory signaling for robust *in vitro* expansion of Tregs was somewhat unexpected as these cells were anticipated to directly proliferate to IL-2 as they constitutively express high amounts of the high affinity IL-2R.

Therapeutically, CD4$^+$ Teff and Treg cells expand along with CD8$^+$ T cells when purified T cells or PBMCs are engineered with chimeric antigen receptors or TCRs (CAR-T) for adoptive cellular therapy (ACT) of cancer.[12–15] Purified Tregs are similarly engineered and expanded for ACT of autoimmune diseases.[16–18] Very similar culture conditions are used to expand human Treg and Teff cells *in vitro* for ACT, which circumstantially suggests that both may use similar molecular programs for expansion. Indeed, proximal TCR signaling is similar in Treg and Teff cells,[19] but some downstream consequences differ. One well-known example is that Teff cells have more robust activation of the PI3K/ATK and mTORC1 pathways, which promote cellular survival and proliferation. This is accounted for because Tregs have higher amounts of phosphatase and tensin homolog on chromosome 10 (PTEN), which limits the PI3K pathway, because TCR signaling in Teff cells is more effective in downregulating PTEN.[20–22] High PTEN lowers TCR and IL-2R signaling in Tregs as both pathways activate PI3K.

The action of PTEN in Tregs raises the distinct possibility that downstream consequences of TCR/CD28/IL-2R-dependent gene activation differs between CD4$^+$ Treg and Teff cells, but the exact nature how this varies is not well understood. Moreover, understanding gene regulation in human Treg and Teff cells as they expand *in vitro* will define intrinsic differences between these cells and may guide approaches to improve them for ACT of autoimmunity and cancer. Other studies have examined gene expression of Treg and Car-T cells, but most examined this at restricted time points and only some studies purified CD4$^+$ Teff cells.[23–28] Here, we directly address this issue by systemically comparing the chromatin landscape and transcriptome of human CD4$^+$ Treg and Teff cells during a 12-day culture period, from culture initiation and initial re-stimulation through the TCR/CD28 and the IL-2R 9-days later. We used identical culture conditions, crosslinking TCR/CD28 with magnetic beads and high IL-2, for both cells populations. When compared to Tregs, Teff cells exhibit heightened gene expression that supports more

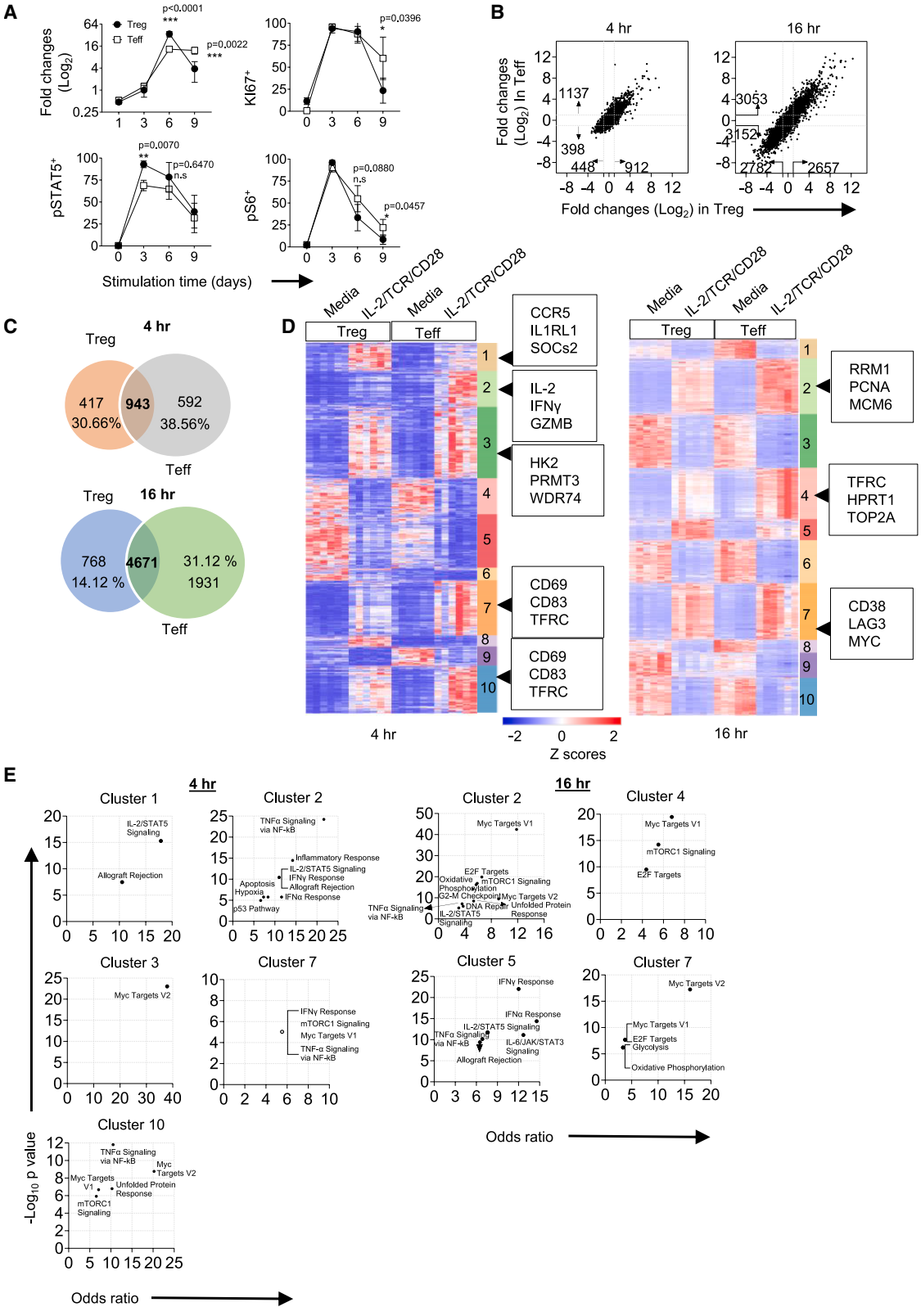

(legend on next page)

robust proliferation. Correspondingly, Tregs showed more rapid contraction and more quickly return toward a state like unstimulated baseline cells, but re-stimulation through the TCR/CD28 and IL-2R reinitiated the Treg proliferative program. These findings are discussed with respect to regulation of Treg and Teff homeostasis and ACT.

RESULTS

Experimental design to explore gene expression of proliferating Treg and Teff cells

To assess the molecular programs controlling the expansion of human Tregs and $CD4^+$ Teff cells *in vitro*, we defined the relative contributions TCR/CD28-and IL-2R-dependent signaling on gene expression and the chromatin landscape over a 12-day culture period (Figure S1). We compared gene expression changes at early time points (4 and 16 h), followed by integration of RNA sequencing (RNA-seq) and assay for transposase-accessible chromatin using sequencing (ATAC-seq) data during more extended culture (days 1–9), and finally assessed the consequences of gene expression when cells were further cultured in IL-2 or re-stimulated through the TCR/CD28/IL-2R (days 9–12). The input cells for these experiments were fluorescence-activated cell sorting (FACS)-purified (typically >95% pure) $CD4^+$ $Foxp3^{neg}$ $CD25^{lo}$ $CD45RA^{neg}$ $CD127^{hi}$ T_{EM} cells and $CD4^+$ $Foxp3^+$ $CD25^{hi}$ $CD127^{lo}$ Tregs, which were mostly $CD45RO^+$ Tregs (81.1% ± 10.2; mean ± SD) (Figure S2). We chose to compare the responses by these two cell populations as both are antigen experienced, Tregs to self-antigens and T_{EM} to exogenous antigens. These cells were stimulated with a combination of anti-CD3/CD28 and IL-2, yielding activated Tregs or Teff cells and they were further expanded from days 3–9 with only IL-2 followed by re-stimulation with anti-CD3/CD28 and IL-2.

The expansion and signaling of Treg and Teff cells were assessed over 9 days after an initial culture with anti-CD3/CD28 plus IL-2 and subsequent passages with only IL-2 on days 3 and 6. Treg and Teff cells showed a similar response on day 3 to TCR/CD28/IL-2R signaling. On day 6 after re-culture with IL-2, Tregs showed greater capacity to expand (2.8-fold) than Teff cells. This is associated with somewhat greater activation of STAT5 by Tregs. However, after that time Teff cells showed equivalent expansion to IL-2 from days 6–9, whereas that of Tregs was reduced (Figure 1A). The expression of the proliferation marker Ki67 largely followed the pattern of expansion of Tregs and Teff cells. Notably, as expected, the activation of pS6 was more sustained in Teff cells, as this latter phase of the cell culture is highly dependent on IL-2 and PTENs tempers IL-2R signaling in Tregs.[21] Thus, the more effective activation of pS6 is likely related to enhanced TCR/CD28/IL-2R signaling upstream of pS6, supporting more prolonged Teff cell expansion.

Early effects of TCR/CD28/IL-2R stimulation of Treg and Teff cells

The gene expression profile of Treg and Teff cells was determined by RNA-seq 4- and 16-h post-stimulation with anti-CD3/CD28 and IL-2. Cells cultured in media served as the control. 1,360 and 1,535 differentially expressed genes (DEGs cutoff: 2-fold change; false discovery rate [FDR] <0.01) were identified in Treg and Teff cells, respectively, at 4 h with the majority being upregulated after stimulation (Figure 1B; Tables S1 and S2). A much greater number of DEGs (5,439, Treg; 6,205, Teff) was seen at 16 h with near equal number of up- and downregulated genes. At both time points, the majority of DEGs were shared between Treg and Teff cells, but some at each time point were uniquely associated with one or the other (Figure 1C).

Hierarchal clustering of normalized transcripts per million (TPM) of 1,881 and 6,984 DEGs that fulfilled the aforementioned cut-off at 4 and 16 h, respectively, were assessed to determine the extent some genes are uniquely regulated in Treg or Teff cells (Figures 1D and S3). At 4 h post-stimulation, most genes within these 10 clusters were co-regulated in Treg and Teff cells, although statistical differences in clusters 1, 2, 3, and 7 were found (Figure S3). Genes in cluster 1, which include CCR5, IL1RL1, and SOCS2, were more upregulated in Tregs compared to Teff cells. In contrast, genes in cluster 2 (including IL-2, IFNγ, and GZMB), cluster 3 (including HK2, PRMT3, and WDR74), and cluster 7 (including CD69, CD83, and TFRC) were more upregulated in Teffs compared to Tregs. Transcriptome changes were significantly different between Treg and Teff for all clusters by 16 h post-stimulation (Figure 1D, right; Figure S3). Genes associated with cell proliferation and activation were strikingly more upregulated in Teff cells in clusters 2, 4, and 7, indicating that gene activation by TCR/CD28/IL-2R signaling was more effective.

Each cluster at 4 and 16 h was examined for enrichment using MSigDB Hallmark pathways. Given the large number of genes in each cluster, we focused on highly enriched pathways ($p_{adj} < 10^{-6}$). At 4 h, genes related to IL-2/STAT5 pathway were most enriched in cluster 1 for Tregs and in cluster 2 for Teff cells (Figure 1E, left). Pathways enriched in clusters 3, 7, and 10, are related to Myc targets, mTORC1 signaling, and several downstream targets of TCR signaling, e.g., interferon gamma (IFNγ) response and tumor necrosis factor alpha (TNFα) signaling via nuclear factor kappa B (NF-κB) (Figure 1E,

Figure 1. Profiling of Treg and Teff after early stimulation of the IL-2R/TCR

(A) Cell expansion, proliferation as asses by Ki67, and activation leading to $pSTAT5^+$ or $pS6^+$ were determined over the 9-day culture period. Data ($n = 4$ biological replicates) are expressed as the mean ± standard deviation and were analyzed by a two-way ANOVA (Sidak's multiple comparison test).

(B–E) The transcriptome of Treg and Teff cells 4 and 16 h after culture initiation ($n = 6$ biological replicates).

(B) Number of DEGs (fold-change $\geq$ Log_2 [1], FDR<0.01) after RNA-seq in relationship to baseline unstimulated cells.

(C) Identification of common and unique significant DEGs.

(D) Hierarchical clustering of DEGs depicting the *Z* scores scaled for 1,881 (4 h) or 6,984 (16 h) genes in Treg and Teff cells where red indicates higher and blue lower expression. Selected clusters and genes are indicated with arrowheads and rectangles, respectively.

(E) The gene ontology (GO) Hallmark2020 pathway enrichment analysis (p_{adj} value $\leq 10^6$) of the genes included in selected clusters from (D) at indicated times. Significance ($-\log_{10} p$ value) of each pathway versus its odds ratio is shown. (ns, non-significant). Also see Figure S3; Tables S1 and S2.

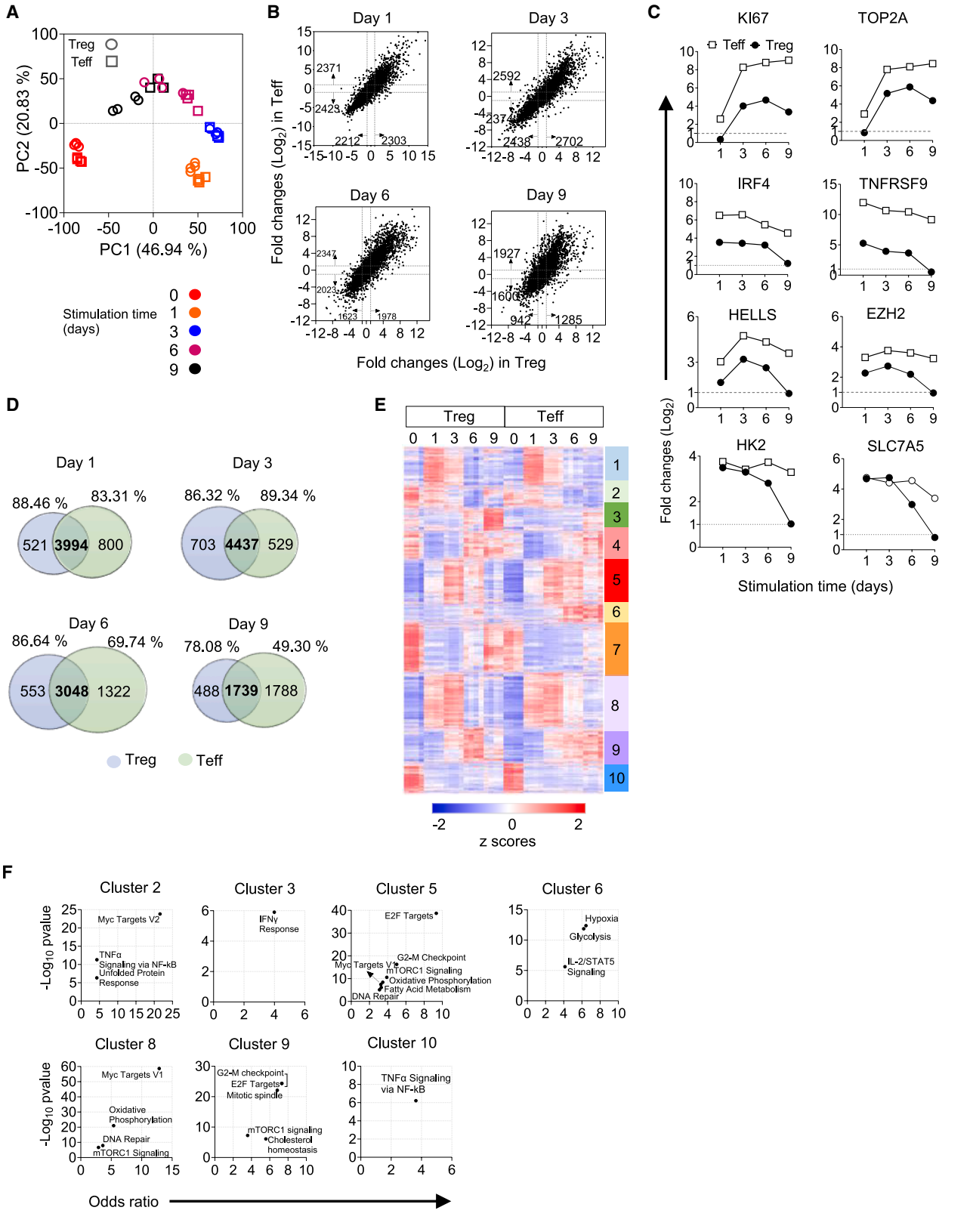

(legend on next page)

left). Many genes in these clusters based on statistical analysis (Figure S3) were more highly upregulated in Teff cells, consistent with somewhat more effective activation of the PI3K and mTORC1 pathway. The other clusters lacked pathways that had high p_{adj} values. At 16 h, clusters 2, 4, 5, and 7 contained highly enriched pathways that overlapped with those found at 4 h (Figure 1E, right). Clusters 2, 4, and 7 not only contained pathways related to Myc targets and mTORC1 signaling but other pathways related to energy metabolism and cell cycle progression. The DEGs in these three clusters were more substantially upregulated in Teff cells. Genes in cluster 5 were more highly expressed in Tregs and were related to several immune processes that may be linked to TCR signaling. Overall, these findings indicate that TCR/CD28/IL-2 signaling leads to a substantial and progressive increase in gene activation and most of these gene targets are co-regulated in Treg and Teff cells, but genes related to mTORC1 signaling and Myc targets were more highly expressed in Teff cells.

Transcriptional changes diverge over time in Treg and Teff after TCR priming and expansion with IL-2

The proliferation patterns of Treg and Teff in response to persistent TCR/IL-2R stimulation peaked at day 6 then diverged (Figure 1A). This result suggests that the transcriptional responses of Treg and Teff cells eventually differ upon stimulation with IL-2. To gain insight into the TCR/CD28/IL-2R stimulation-induced transcriptional changes longitudinally across time, RNA-seq was performed for Treg and Teff cells at days 1, 3, 6, or 9 post-activation with TCR/CD28/IL-2R signaling and expansion in IL-2. These data were compared to the transcriptome of the baseline input cells without stimulation. Principal-component analysis (PCA) revealed that time post-stimulation was an important driver of transcriptional changes. In reference to the unstimulated cells, the pattern in the PCA moved in a counterclockwise manner. The transcriptomes of Treg and Teff cells at days 1 and 3 post-stimulation were grossly similar and differed the most when compared to baseline. After that time, the transcriptome of Treg and Teff cells moved back toward baseline and this effect was most striking for Tregs (Figure 2A). DEGs in relationship to baseline were also identified for Treg and Teff cells over this period (Figure 2B; Table S3). Pairwise comparison of DEGs showed that TCR/CD28/IL-2R signaling elicited a similar transcriptional response in Treg and Teff cells on days 1 and 3, which peaked at day 3. After that time, fewer DEGs were found for Tregs. Genes bearing this pattern include proliferation-associated Ki67 and TOP2A, TCR responsive IRF4 and TNFRSF9, heterochromatin regulators HELLS and EZH2, and metabolism-associated HK2 and SLC7A5. These were initially upregulated, but often at a higher amount in Teff (Figure 2C). By day 9, when compared to Teff cells, these transcripts were more substantially downregulated in Tregs, and several were expressed at levels like baseline. These findings suggest that after initial activation through TCR/CD28/IL-2R, the proliferative potential to expand to IL-2 is programmed to decrease, and this process proceeds more rapidly for Tregs.

In line with samples distribution according to PCA, the number of DEGs that overlap between Treg and Teff was highest on days 1 and 3 and then decreased on days 6 and 9. This decrease in overlapping DEGs resulted in more transcripts that were distinct for Teff cells (Figure 2D). Hierarchical clustering was performed for transcripts across all time points, where one or more time points contained a DEG (Figure 2E). Pathway analyses of genes within each cluster was also performed and seven clusters were identified with significant enrichments (p_{adj} at least $<10^{-6}$) (Figure 2F; Table S3).

Treg and Teff cells exhibited a similar pattern of gene expression for 5 clusters (clusters 1, 2, 4, 8, and 10), consistent with co-regulation as they respond to anti-CD3/CD28 plus IL-2 priming and subsequent expansion to IL-2 (Figure 2F). Cluster 8 was enriched in pathways related to Myc targets, oxidative phosphorylation, DNA repair, and mTORC1 signaling, indicative of pathways related to activation and gene expression supporting proliferation. For the other 4 clusters, Treg and Teff cells showed distinctive gene expression on one or more days. The genes that mapped to cluster 3 at baseline and especially on day 9 showed much higher expression in Tregs. This cluster included genes associated with Treg lineage, such as FOXP3, LRRC32, and IKZF2 (Helios), suggesting that the Treg lineage may be reinforced. Cluster 3 also includes IFN-associated genes, such as IFI35, IFIT3, IRF1, and IRF9. IFN-associated genes were also highly enriched in Tregs, but not Teff cells, 16 h after stimulation with TCR/CD28/IL-2 (cluster 5; Figures 1D and 1E). In contrast, cluster 6 and 9 includes genes upregulated at days 6 and 9, or day 9, respectively, only in Teff cells. Pathways highly enriched in cluster 6 include hypoxia and glycolysis and cluster 9 include G2-M checkpoint, E2F, mitotic spindle, mTORC1 signaling and cholesterol homeostasis. This finding is consistent with the ability of Teff cells to show continued expansion to IL-2 from days 6–9. Collectively, all these data indicate that the longer duration of Teff cell expansion is due to more robust gene expression, especially those genes associated with mTORC1, energy metabolism, and cell cycle progression.

Figure 2. TCR/CD28/IL-2R signaling induces transcriptional changes that result in a greater long-term expansion of Teff cells

(A) Principal-component analysis (PCA) of normalized RNA-seq data as transcripts per million (TPM) of the Treg and Teff cells.

(B) Number of DEGs (fold-change $\geq$ Log_2 [1], FDR<0.01) elicited in Treg and Teff cells upon stimulation relative to unstimulated cells.

(C) Fold changes of selected statistically significant DEGs (FDR<0.01) from Treg and Teff cells relative to unstimulated cells determined by RNA-seq. Reference dotted line indicates $\geq$ Log_2 [1] change threshold.

(D) Identification of common and unique significant DEGs derived from (C).

(E) Hierarchical clustering depicting the *Z* scores scaled for 11106 TPM before and after TCR/IL-2R stimulation in Treg and Teff cells (red indicating higher and blue lower expression).

(F) The gene ontology (GO) Hallmark2020 pathway enrichment analysis of the genes in selected clusters (p_{adj} value $\leq 10^6$) from (F). Significance (-log_{10}pvalue) of each pathway versus its odds ratio is shown.

Data (A)–(F) are from 4 independent biological replicates. Also see Table S3.

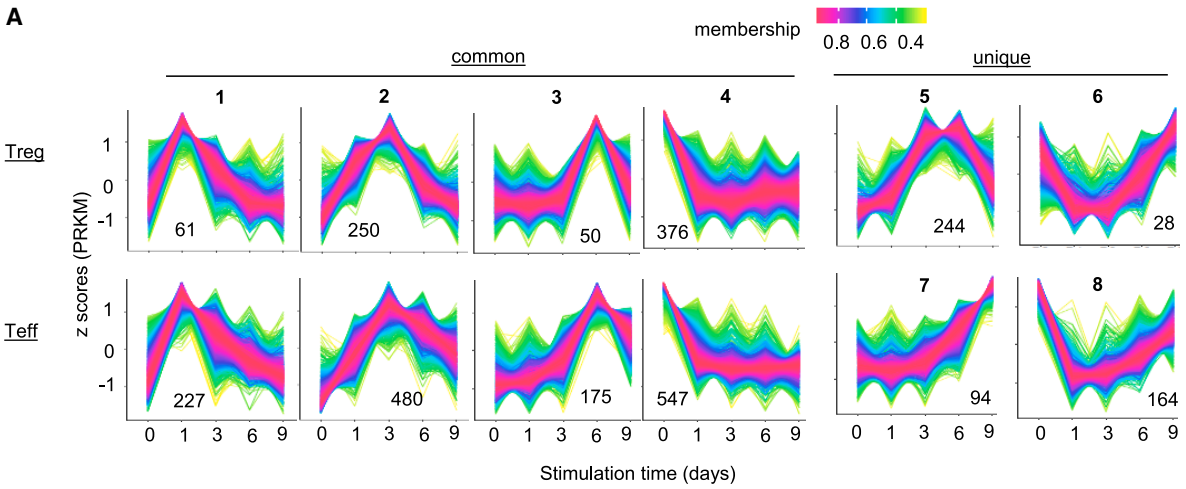

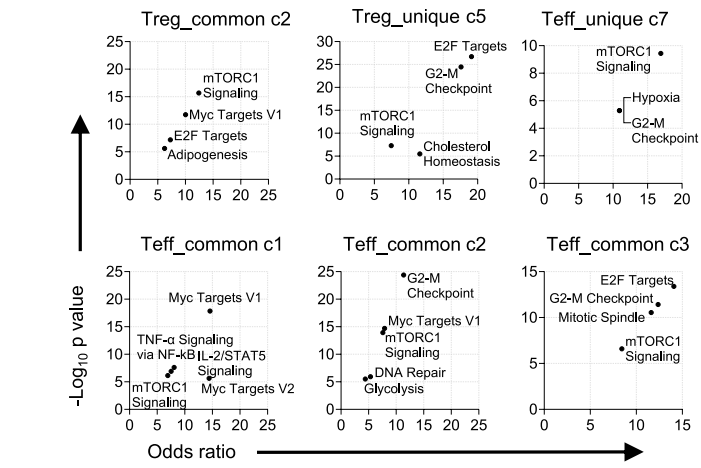

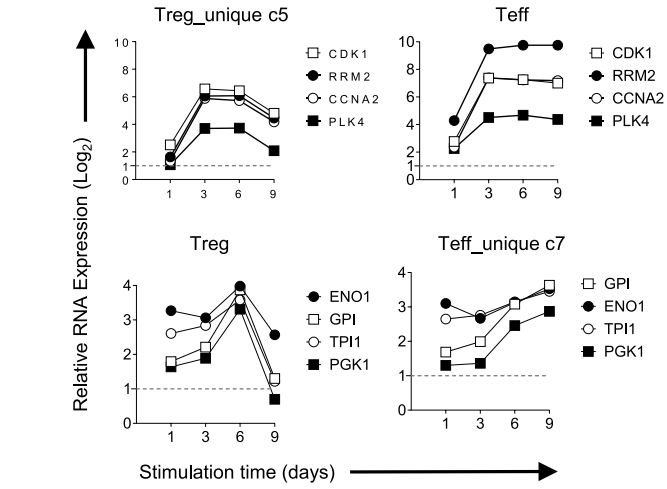

(legend on next page)

Temporal clustering of DEGs between Treg and Teff cells

The preceding analysis represents a static view of gene expression in Treg and Teff cells as they respond after activation and subsequent expansion to IL-2. We next determined whether transcriptional changes after stimulation had unique temporal patterns by performing k means clustering between time points. Six patterns were chosen as the minimal number capturing different patterns and are ordered according to the time when the peak of upregulation is reached. Patterns 1–4 captured similar gene expression between Treg and Teff cells (Figure 3A; Table S4). Comparatively, a larger number of DEGs was noted on each common pattern for Teff cells. The DEGs included in patterns 1–3 reached their peaks at days 1, 3, or 6, respectively. In contrast, DEGs in pattern 4 are persistently downregulated upon stimulation of baseline cells and include the largest number of DEGs for each cell type, indicating that many genes in unstimulated Treg and $CD4^+$ T conventional cells were downregulated because of TCR/CD28/IL-2R signaling.

Pathway analyses of DEGs within each pattern was also performed and 6 patterns, 2 for Tregs and 4 for Teff cells, were identified that contained significant enrichments (p_{adj} at least $<10^{-6}$) (Figure 3B). All six patterns are associated with pathways that support cellular activation (MTORC1, Myc targets, E2F) and proliferation (G2M checkpoint, mitotic spindle). Patterns 2 and 5 in Tregs are related to these pathways with peak gene expression on days 3 and 6, whereas patterns 1, 2, 3, and 7 for Teff cells are related to peak gene expression on days 1, 3, 6, and 9. This result is also consistent with more efficient activation of conventional $CD4^+$ T cells through stimulation with anti-CD3, anti-CD28, and IL-2, as well as more prolonged expansion in response to IL-2.

To illustrate this point, the time course of several DEGs is shown for unique pattern 5 in Tregs or unique pattern 7 in Teff cells (Figure 3C) and compared to those genes in Teff and Treg cells, respectively. The E2F targets, CDK1, RRM2, CCNA2, and PLK4, associated with proliferation in cluster 5, are upregulated at days 3 and 6 in Tregs and then downregulated, a pattern that coincides with maximal Treg expansion on day 6 (Figure 2A). Glycolysis-associated genes, GPI, ENO1, TPI, and PGK, were upregulated from day 6 onward. This finding suggests that the more persistent proliferation by Teff cells is in part related to more sustainable upregulation of not only proliferative genes but also those related to metabolic processes.

Dynamic temporal chromatin remodeling in Treg and Teff cells after TCR priming and expansion with IL-2

As RNA expression is dependent upon DNA accessibility, we sought to define the dynamics of chromatin landscape changes in human Treg and Teff cells after priming and subsequent expansion with IL-2 and characterize the intersection of these changes with the transcriptome data obtained by RNA-seq. Here, DNA was obtained from the same cultures as used for RNA-seq. Notably, RNA-seq revealed DEGs of chromatin remodelers with distinct patterns of expression in Treg and Teff cells, supporting the notion of some distinct temporal effects on the chromatin landscape of Treg and Teff cells. As examples (Figure 4A; Table S3), SMARCB1 contributes to repressive chromatin structures.[29] ARID5A stabilizes TBX21 mRNA that will affect gene expression, to enhance IFNγ transcription and secretion.[30] SUV39H1 and DNMT3b, a histone methyl transferase and a DNA methylase, respectively, limit gene expression.[31,32]

Analogous to the transcriptome data (Figure 2A), PCA of the chromatin landscapes of Treg and Teff cells after ATAC-seq at each time point revealed a clockwise movement, indicating that time was an important driver of chromatin accessibility patterns. The largest divergence of the chromatin landscape from baseline unstimulated cells (upper left quadrant) was noted at day 3 for both cell populations and then they reverted toward the unstimulated cells at day 9 (Figure 4B). These changes in chromatin accessibility were dominated by an increase in chromatin accessibility for both Treg and Teff cells and was most noticeable at days 3 and 6 (Figure 4C). Most differential accessible regions (DARs) mapped to intronic regions followed by intergenic regions at all time points (Figures 4D; Table S5). As examples, sequencing tracks annotated to IL2RA, IKZF4, FOXP3, and IFNγR2 illustrate chromatin accessibility that occurred during activation and expansion of Treg and Teff cells (Figure 4E).

HOMER was used to identify *de novo* enriched TF motifs in the DARs that may contribute to gene expression, where the top 5 are shown in Figure 4F. The top motif enrichments were distinct between Treg and Teff cells especially on day 1. BATF (Basic Leucine Zipper ATF-Like Transcription Factor), a transcription factor implicated in the epigenetic and transcriptional programs of activated Tregs[33,34] was the top enriched motif for Tregs. In contrast, FRA1, a transcription factor controlling proliferation, differentiation, apoptosis, and immune responses[35] was a dominant motif at most time points for both cells. With respect to Teff cells, two members of the erythroblast transformation-specific family of transcriptions factors, ERG1 and Fli1, which promote Th1 and Th17 function[36,37] were the top enriched motifs (Figure 4F). Overall, these data not only show large overlapping but also some distinct effects on the chromatin landscape in Treg and Teff cells during their activation and expansion *in vitro*.

These ATAC-seq data were subjected to k means clustering between time points to elucidate common and distinct temporal patterns of chromatin changes in Treg and Teff cells (Figure 5A; Table S6). Four out of six clusters exhibited considerable similarity between Treg and Teff cells, indicating that the dynamics of many chromatin changes were independent of cell type. Patterns 1–3 all showed initial opening of DARs, but following this opening each showed a distinct pattern of closing. Pathway analysis of genes associated with these changes in the

Figure 3. Partially overlapping temporal cluster in transcriptional changes in Treg and Teff cells

(A) DEGs from RNA-seq data of Treg and Teff cells were subjected to time course clustering (TCseq). Membership scores, representing the likelihood of a peak being in a specific cluster, are indicated by a color code.

(B) Peak sets with membership scores >0.8 were analyzed for gene ontology (GO) Hallmark2020 pathway enrichment. Clusters with GO enrichments that were highly significant (p_{adj} value at least $<10^{-6}$) are shown.

(C) Fold changes of statistically significant DEGs (FDR<0.01) are shown for unique cluster 5 in Tregs and unique cluster 7 in Teff cells. Also see Table S4.

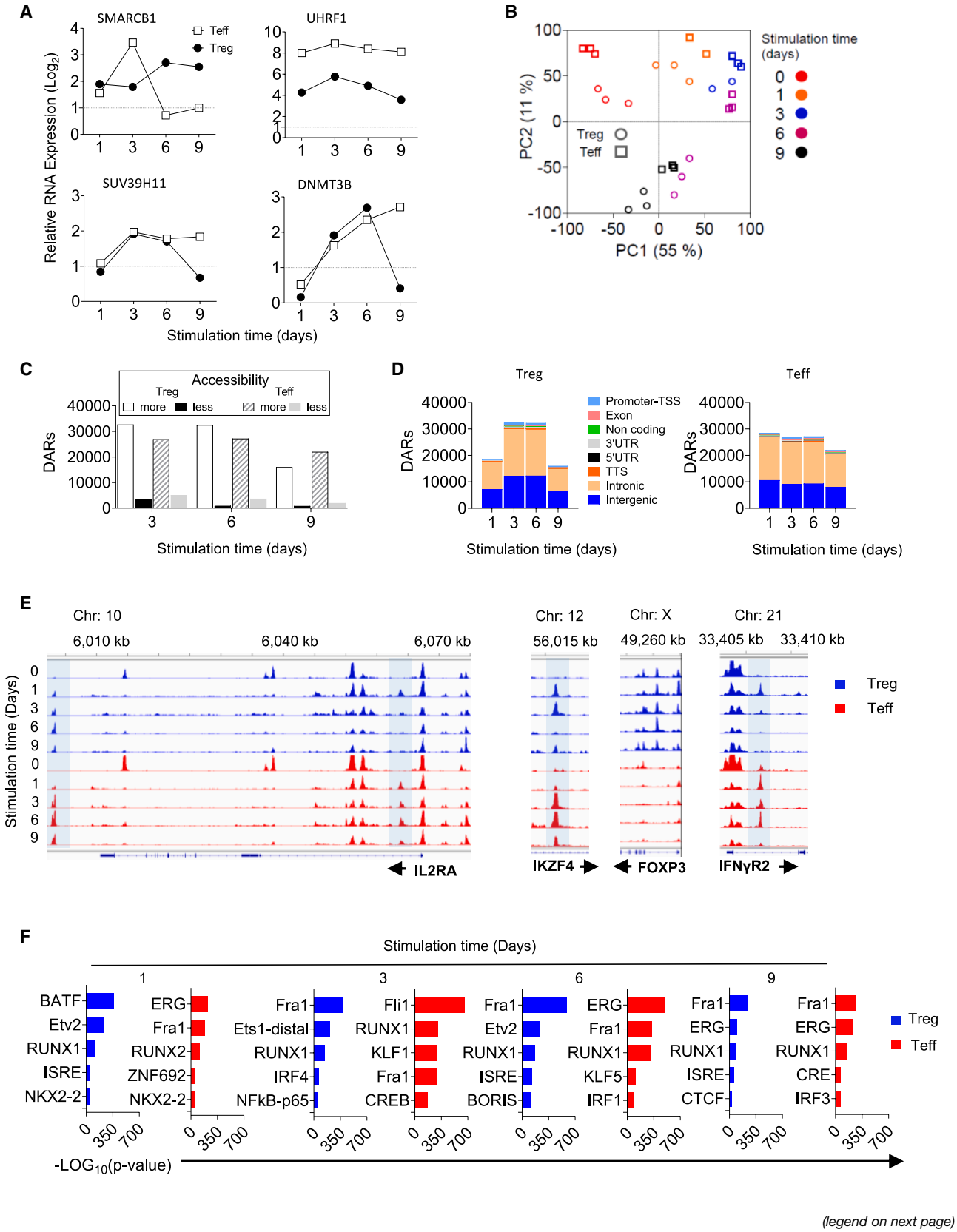

(legend on next page)

chromosomal landscape also revealed sharing that was particularly notable for pattern 3. Patterns 1 and 2 are linked to pathways associated with IL-2/STAT5 signaling whereas pattern 3 is related to pathways important for cell division. These findings further reinforce the idea that activation and expansion of Treg and Teff cells use a highly overlapping mechanism that affects the chromosomal landscape to affect gene expression.

Despite this commonality, Tregs showed several unique changes. Although pattern 4 is shared by Treg and Teff cells, only Tregs contained a relatively high number of DARs (Figure 5A). Pattern 4 initially moves toward closed DARs, but these then open like baseline-unstimulated cells by day 9. Pattern 5, unique to Tregs, revealed DARs that after initial opening and closing, also revert to that of unstimulated Tregs. Pathways associated with patterns 4 and 5 are related to IL2/STAT5 and mTORC1 signaling vs. G2M checkpoint and Myc targets, respectively (Figure 5B). These changes likely contribute to more rapid contraction of Tregs than Teff cells after IL-2-dependent expansion. Patterns 7 and 8 were unique to Teff cells but show similarity to patterns 1 and 4. Genes associated with these patterns in chromosomal changes were also related to the IL-2/STAT5 and mTORC1 signaling as well as TNFα signaling via NF-κB and apoptosis, which may contribute to their more persistent expansion to IL-2 from days 6–9.

Locus overlap analysis (LOLA) was employed to infer the enrichments of transcription factors (TFs) from the ENCODE database (Figure 5C; Table S7) or histone modifications and DNA methylation sites from the Roadmap epigenomics database (Figure 5D; Table S8). These analyses query our DARs with findings from others that have identified TFs or other chromatin remodelers as binding to DNA within these regions of altered chromatin accessibility. Accordingly, this analysis provides support that TF motifs or chromatin modifiers associated with DARs may be functionally relevant.

For patterns 1 and 2, members of the AP-1 transcription factor family, including c-FOS (cellular homolog of the FBJ murine osteosarcoma viral oncogene Fos), JUN (jun proto-oncogene, cellular homolog of the avian sarcoma virus 17 oncogene v-jun), and BATF, were broadly enriched in Treg and Teff cells (Figure 5C). For pattern 3, these DARs exhibited significant enrichments for TFs associated with RNA transcription (POL2 and TAF1) and histone modifications (PHF8 and PLU1). Pattern 4, with many DARs associated only with Tregs, also displayed members of the AP-1 transcription factor family. Patterns 5 and 6, unique to Tregs did not reveal enrichments for TFs, whereas patterns 7 and 8 in Teff cells exhibited enrichments for AP-1 family members, IRF-2, and BCL11A. Histone modifiers with potential to bind DARs varied across each pattern, with some showing enrichment for marks associated with active transcription and others associated with repression (Figure 5D). Collectively, our data demonstrate not only substantial overlap in chromatin accessibility and utilization of TFs and chromatin modifiers but also temporal differences as Treg and Teff cells response to TCR, CD28, and IL-2R signaling. Many of these changes facilitate transcription and gene expression associated with cell expansion. However, accessibility reduction to their binding motifs for proliferation-associated transcription factors in Treg, but not Teff cells, may contribute to the observed variations in expansion kinetics between these cells.

Distinct metabolic re-programming in Treg and Teff cells after TCR priming and expansion with IL-2

Cell growth and function rely on adequate energy generation and biosynthesis of precursors to synthesize larger macromolecular complexes. Considering the distinct kinetics of expansion and chromatin remodeling observed in Treg and Teff cells (Figures 2A and 4C) and that genes related to glycolysis and oxidative phosphorylation were upregulated to a greater amounts in Teff cells (Figures 1D and 3B), we hypothesized that activation and IL-2-dependent expansion in Treg and Teff cells would distinctly modulate transcriptome programs that affect metabolic networks to meet the energy requirements of cell expansion and epigenetic remodeling.

Our unbiased analyses (Figures 2G and 3D) revealed DEGs related to oxidative phosphorylation and glycolysis in several clusters. Hierarchical clustering, therefore, was performed for 317 genes from our RNA-seq data that are members of the glycolysis and oxidative phosphorylation HALLMARK gene set collections (Figure 6A; Tables S3 and S9). Clusters 2 and 6 encompass sets of genes that were more highly expressed in Teff cells than in Tregs on day 9. These genes included PKM, HK2, LDHA, TPI1, ENO1, and GPI (Figure 6B), important components of the glycolytic pathway. Subsequently, we investigated whether these types of cell-specific changes reflected the re-programming of metabolic pathways. The oxygen consumption rate (OCR), an indicator of oxidative phosphorylation (OXPHOS), and the extracellular acidification rate (ECAR), a consequence of lactic acid production and a marker of glycolysis were measured under basal conditions and after the addition of mitochondrial respiration modulators. Oligomycin, FCCP (carbonyl cyanide-p-trifluoromethoxyphenylhydrazone), and rotenone/antimycin A were added to non-stimulated cells and at indicated times following TCR/CD28/IL-2R priming and IL-2-dependent expansion. The transition from basal to stressed metabolic activity

Figure 4. Dynamics of chromatin accessibility changes in Treg and Teff cells

(A) Expression profiles of statistically significant DEGs (FDR<0.01) for several chromatin remodelers derived from RNA-seq. Reference dotted line indicates ≥ Log_2 [1] change threshold.

(B) Principal-component (PC) analysis of normalized ATAC-seq data according to their length. Percentages of variation are shown in parentheses.

(C) Pairwise comparison accessibility (stimulated vs. unstimulated: more accessible = fold-change ≥ [1.5]; less accessible = fold-change ≤ [1.5]) of significant (p value < 0.05) differentially accessible regions (DARs) in Treg and Teff cells.

(D) Number and genomic distribution of DARs identified by ATAC-seq in each cell type. Genomic annotations included the promoter-transcription starting site (TSS) (≤3 kb), exon, non-coding, 3′-UTR, 5′-UTR, transcription termination site (TTS), intronic, and intergenic regions.

(E) Genome browser snapshots showing the ATAC-seq signal at the indicated some representative loci. Regions more accessible after TCR/IL-2R stimulation are highlighted by light blue bars.

(F) Top 5 motifs after HOMER *de novo* motif analysis for promoter regions (≤3 kb from TSS) of open sites in Treg and Teff. Also see Tables S3 and S5.

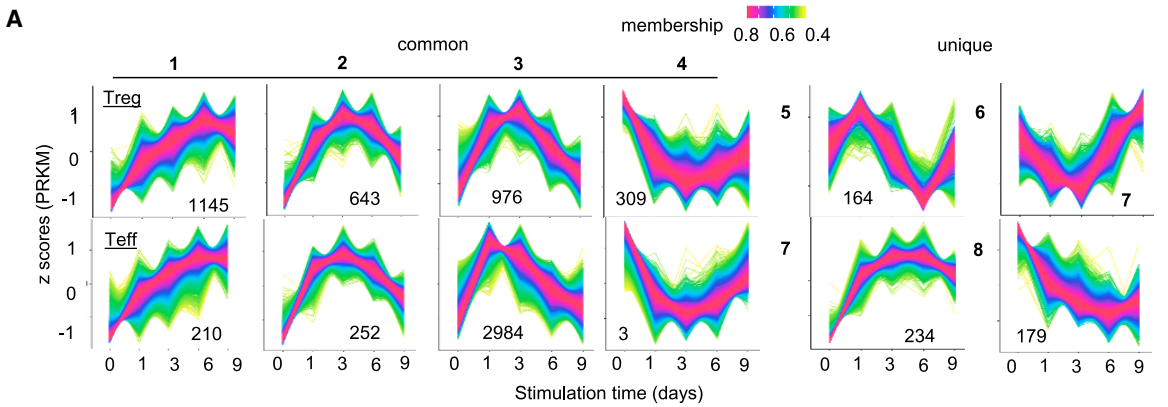

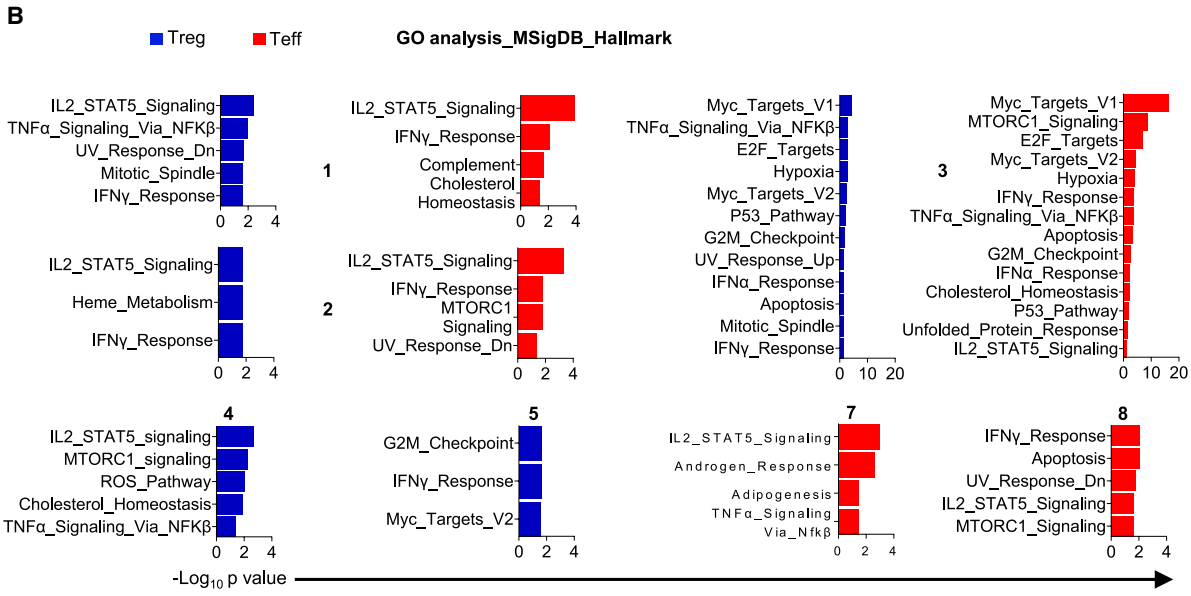

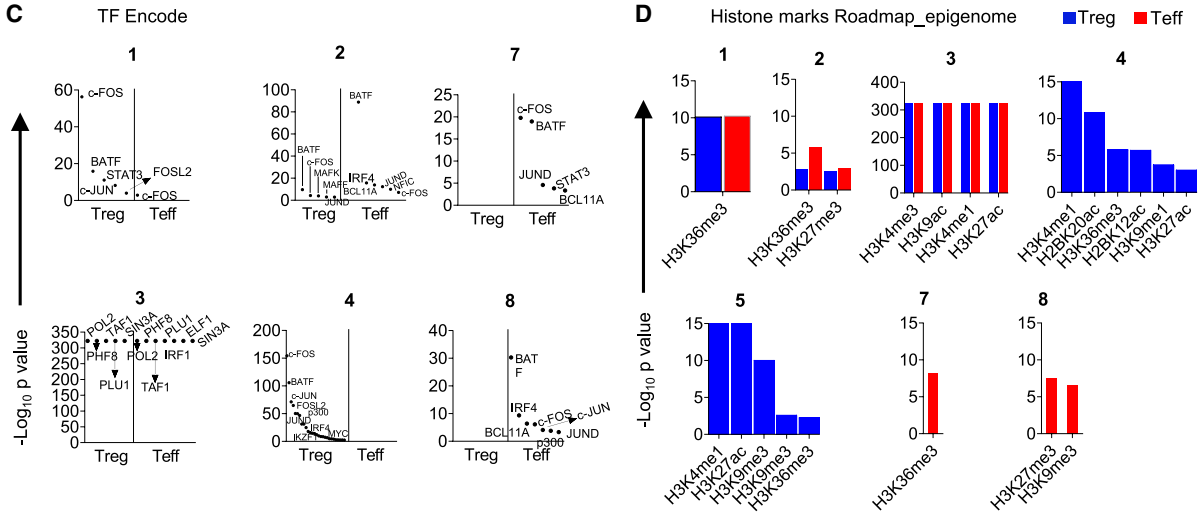

(legend on next page)

after the injection of inhibitors represents the metabolic potential of Treg and Teff cells.

Basal metabolic activities based on OCR and ECAR readouts were low in unstimulated Treg and Teff cells, albeit significantly higher in the latter. Additionally, Treg and Teff cells initially exhibited low oxygen consumption, yet Teff cells demonstrated a superior ability to respond to increased energy demand compared to Tregs (Figure 6C). After stimulation, the basal levels of OCR in Teff cells were higher at day 3, whereas ECAR values were higher only at day 9. Responses to mitochondrial modulators were consistent throughout the experimental time frame, except at day 9, when a notably larger increase in the ECAR value in response to the addition of oligomycin was observed exclusively in Teff cells (Figure 6D). Lastly, we compared cellular energy phenotyping for Treg or Teff cells to assess whether a metabolic shift toward more aerobic or glycolytic activity occurred during their activation and expansion (Figure 6E). In unstimulated cells, Teff cells displayed a more energetic phenotype than Tregs, whereas they both similarly increased their aerobic (mitochondrial) and glycolytic potentials when evaluated on days 3 and 6. However, on day 9 Tregs shifted toward a more quiescent state while Teff cells still exhibited a more energetic phenotype. This more energetic activity by Teff cells likely contributes to their more prolonged IL-2-dependent expansion after priming with anti-CD3/CD28 plus IL-2.

Treg expansion re-ensues after re-engaging TCR/CD28/IL-2R signaling

Unlike Teff cells, Tregs exhibited significantly reduced proliferation capabilities after 9 days in culture with IL-2 (Figure 2A). This result coincides with lower numbers of DEGs (Figures 2B; Table S3), DARs (Figures 4C; Table S5), and a less energetically active phenotype (Figure 6E). Furthermore, using *Z* score analysis for activation (active ≥ 2; inhibited ≤ -2), a side-by-side comparison of DEGs at day 9 with ingenuity pathway analysis (IPA) predicted significantly enhanced activities in Teff cells. They include translation regulation (LARP1), co-stimulatory signals (CD28), transcription regulation (ETV3, ETV6, FOXO1, NFATC2, IKBKB, KAT2B, KDM8, and KDM4B), the cytokine IL-2, cell surface receptors (CD3 and TREM1), the cell cycle regulator RB1, and canonical pathways related to biosynthesis of DNA/RNA precursors and amino acids. (Figure 7A). These findings indicate that after contraction between days 6–9, Tregs at day 9 are less responsive to IL-2 than Teff cells.

We hypothesized that re-engaging the TCR/CD28/IL-2R pathways in Tregs would enhance gene expression and support proliferation. To test this hypothesis, day 9 Treg and Teff cells were re-stimulated with IL-2 or anti-CD3/CD28 plus IL-2 and cell expansion as well as STAT5 activation were determined. As expected, Tregs minimally expanded to IL-2 but showed proliferation that is more robust upon re-stimulation with anti-CD3/CD28 plus IL-2. (Figure 7B). This latter expansion by Tregs was like that for Teff cells after culture with IL-2 or anti-CD3/CD28 plus IL-2. We wish to emphasize the expression of *Foxp3* mRNA remained high for Tregs, but low for Teff cells, throughout the 12-day culture period, indicating that contaminating Teff cells cannot explain the response by Tregs to re-stimulation by anti-CD3/CD28 plus IL-2. (Figure S4). Expression of Ki67 generally followed this pattern of cell expansion. Both cell populations showed similar activation of STAT5. This result indicates that Treg cells are more dependent on TCR/CD28 for continued expansion than Teff cells. Moreover, Teff cells are distinctively programmed to develop more persistent expansion to IL-2.

The transcriptomes of Treg and Teff cells were assessed on day 12 for the same cells that expansion was measured after re-stimulation with IL-2 or anti-CD3/CD28 plus IL-2. RNA expression was compared to input baseline unstimulated cells. With respect to re-stimulation with only IL-2, fewer DEGs were noted for Tregs (2,930 DEGs) than Teff cells (4,446) (Figure 7C; Table S10). This finding is consistent with fewer DARs in Tregs at day 9 (Figure 4C). In contrast, a similar number of DEGs were noted for Treg and Teff cells after re-stimulation with anti-CD3/CD28 plus IL-2 (Figure 7C), consistent with similar cell expansion (Figure 7B).

To explore these transcriptional changes in Tregs associated with their expansion, we compared DEGs in Tregs after stimulation with only IL-2 or anti-CD3/CD28 plus IL-2 (Figure 7D). Most genes overlapped between these two culture conditions, but 41.7% of the DEGs (1,921) were distinctively associated after TCR/CD28/IL-2R signaling. Further analysis focused on these 1,921 DEGs as these may provide clues why only anti-CD3/CD28 plus IL-2 supported expansion of Tregs. IPA predicted heightened expression of genes related to cell proliferation, particularly the mitotic metaphase and anaphase pathway with the highest enrichment score (Figure 7E). Generic transcription was the top inhibited pathway. Additional comparison of enriched canonical pathways for Treg and Teff cells after both re-stimulation conditions also revealed that the generic transcription pathway was significantly enriched and inhibited for all conditions that lead to Treg or Teff expansion (Figure S5).

When the 1,921 DEGs were overlaid on the generic transcription pathway, IPA revealed marked differences in expression for several members of transcriptional repressors (e.g., CKRAB-ZNF/KAP) or coactivators (e.g., PCAF, TRAP, and CSL-NICD) complexes when comparing Tregs stimulated with only IL-2 vs. anti-CD3/CD28 plus IL-2 (Figure 7F). Treg expansion by the latter was associated with increases in

Figure 5. Temporal clustering in chromatin accessibility partially overlap in Treg and Teff cells

(A) Peak sets from ATAC-seq data of Treg and Teff cells before and after TCR/IL-2R stimulation were generated and subjected to time course sequencing clustering (TCseq). Membership scores, representing the likelihood of a peak being in a specific cluster, are indicated by a color code.

(B) Peak sets with membership scores >0.8 were analyzed for gene ontology (GO) Hallmark2020 pathway enrichment. Clusters with GO enrichments that were highly significant (p_{adj} value at least $<10^{-6}$) are shown.

(C and D) Transcription factor binding site (TFBS) prediction or histone marks enrichments according to the ENCODE database (C) or Roadmap epigenome database (D). The peak sets with membership scores >0.8 from the TC analysis were used. Each dot (C) or bar (D) represent the significance (-log10pvalue) on Treg or Teff. Also see Tables S6, S7, and S8.

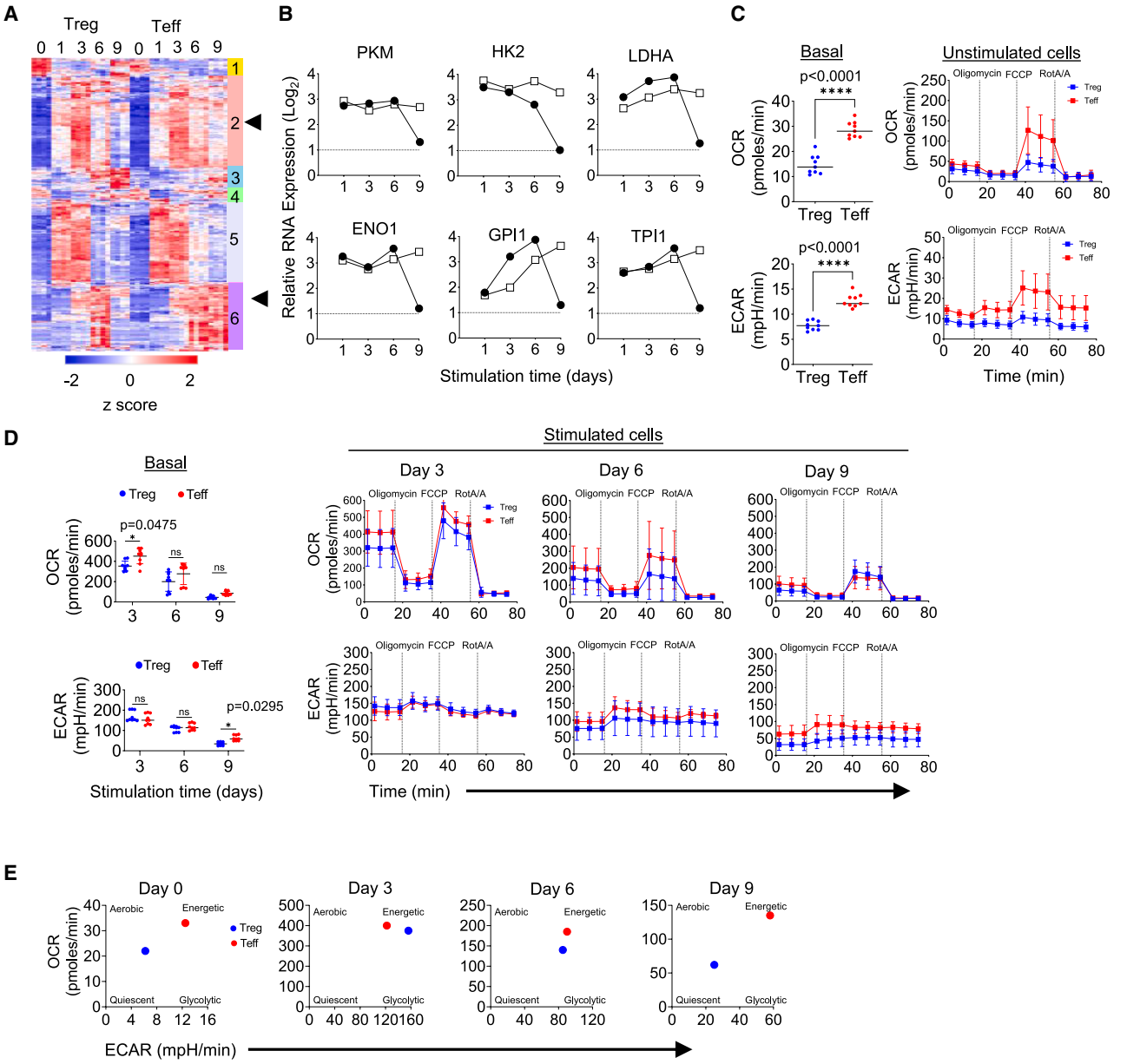

Figure 6. Distinct metabolic re-programming in Treg and Teff cells after TCR priming and expansion with IL-2

(A) Hierarchical clustering depicting the *Z* scores scaled of 317 transcripts (normalized transcripts per million (TPM) derived from RNA-seq data and identified as members of the GO terms: glycolysis or oxidative phosphorylation. Red indicates higher and blue lower expression, respectively.

(B) Expression profiles of statistically significant DEGs (FDR<0.01) for several glycolytic enzymes found in clusters 2 or 6. Reference dotted line indicates $\geq$ Log_2 [1] change threshold.

(C and D) Treg and Teff unstimulated cells were used to assess metabolic activity by Seahorse analyses. Oxygen consumption (OCR) and extracellular acidification (ECAR) rates were measured under basal conditions and in response to indicated mitochondrial modulators. Data (n = 9, (3) biological replicates x (3) technical replicates are expressed as the mean ± SD and were analyzed by a two-way ANOVA using the Tukey's multiple comparison test); ns, non-significant.

(E) Energy maps for Treg and Teff cells after the indicted culture period. Raw data were analyzed using Seahorse Wave Software (version 2.6.0) prior to graphical presentation using GraphPad Prism version 10.2.3. Also see Tables S3 and S9.

KRAB-zinc finger proteins, which have transcriptional repressor activity, and the TRAP coactivator complex, whereas decreases were observed in the P300/CBP-associated factor (PCAF) coactivator and the CSI-NICD coactivator complex. In summary, anti-CD3/CD28 plus IL-2 re-stimulation of Treg and Teff cells and IL-2-only re-stimulation of Teff cells induced a re-programming of their transcriptomes that included upregulation of potent transcriptional repression complexes to likely facilitating re-engagement in genes necessary for proliferation and expansion.

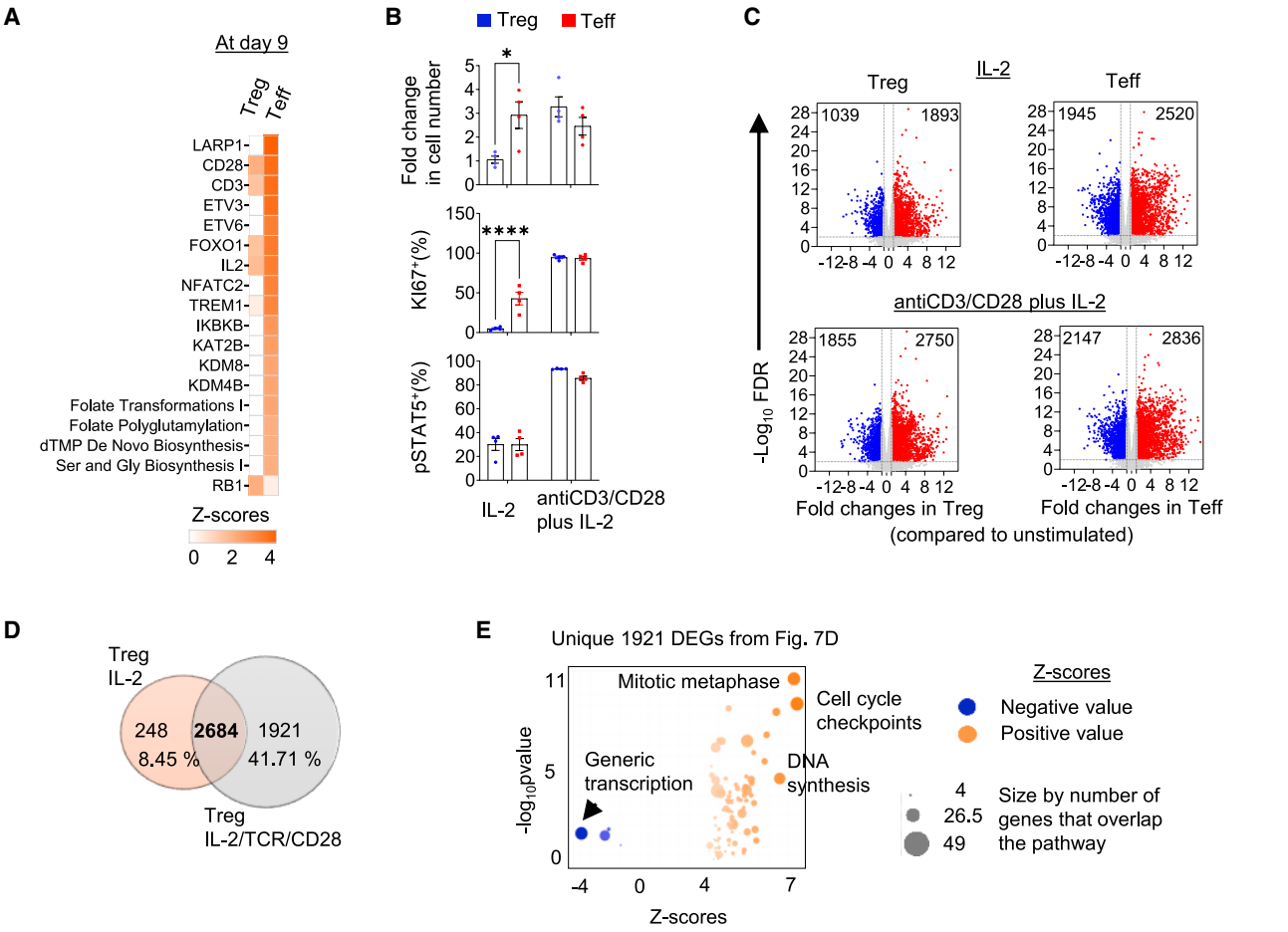

Figure 7. Treg expansion re-ensues after re-engaging TCR/CD28/IL-2R signaling

(A) Ingenuity pathway analysis predicted differences in several activities based on *Z* scores after nine days between Treg and Teff.

(B) Expansion, proliferation as measured by expression of Ki67, or activation of STAT5 was determined for Treg and Teff cells after day-9 cells were stimulated for 72 h with rhIL-2 or anti-CD3/CD28 beads plus rhIL-2. Data ($n = 3$ biological replicates) are shown as the mean ± SD and evaluated with two-way ANOVA by Sidak's multiple comparison test (*$p < 0.0128$ and ***$p < 0.0001$).

(C) RNA was isolated from the day-12 re-stimulated cells and their transcriptomes were determined by RNA-seq. Number of significant DEGs (FDR<0.01, fold change ≥ Log_2 [1]) that were upregulated (red dots) or downregulated (blue dots) are shown.

(D) Identification of common and unique significant DEGs.

(legend continued on next page)

DISCUSSION

In this study, we compared the proliferative activity of Treg and Teff cells and the underlying molecular basis of these responses. Cultures were initiated with purified $CD4^+$ Treg and T_{EM} cells, as both population at baseline are antigen-experienced, Tregs to self-antigen and Teff to nominal antigens. The initial expansion by both cell types was similar after priming with anti-CD3/CD28 plus IL-2 whereas Tregs expanded to a greater level after the first passage using only IL-2. However, after that time Tregs contracted while $CD4^+$ Teff cells continued to show robust responsiveness to a second and third passage with only IL-2.

Our molecular profiling showed substantial overlap in gene expression over the 9-day culture period between Treg and Teff cells as they respond to TCR, CD28 and IL-2R signaling. This finding is not surprising since both cells go from a relatively quiescent state to one of high proliferation. Nevertheless, we uncovered several features that likely contributed to the distinct expansion kinetics by Treg and Teff cells. The more persistent expansion by $CD4^+$ Teff cells is likely multifaceted. One feature is that the temporal upregulation of gene expression is more robust in $CD4^+$ T_{EM} cells, consistent with more effective gene activation in Teff cells than Tregs. In addition, chromatin remodeling in Teff cells, albeit somewhat lower than in Tregs, remained open for a longer time frame. This effect was associated with a subset of genes that were upregulated only between day 6 and 9 for Teff cells. These genes (Figure 2F, cluster 6) are highly linked to pathways related to glycolysis, mTORC1, Myc-targets, and IL-2/STAT5 signaling. Indeed, direct analyses revealed that $CD4^+$ Teff cells exhibited a higher energetic profile and more persistent activation of pS6, downstream of mTORC1, than Tregs. PTEN is downregulated by TCR signaling in Teff cells whereas its level remains high in Tregs, which acts to decrease PI3K/mTORC1 signaling in Tregs.[38] Thus, IL-2R-dependent PI3K/AKT/mTORC1 signaling will be more active in Teff cells as they are continually passaged in IL-2. Correspondingly, Teff cells are also more susceptible to inhibition by rapamycin than Tregs,[39,40] further illustrating the importance of the mTORC1 pathway in Teff cells.[41]

As temporal gene activation in Teff cells by TCR, CD28, and IL-2R signaling led to a high number of genes with coordinated up and downregulation of gene expression, we were surprised that Tregs expanded to a higher amount (2.8-fold) than Teff cells after the first passage in IL-2. We noted that STAT5 activation was higher in Tregs from day 3 through day 9 and that pS6 signaling was similar on day 3 for these two cell populations. These effects are associated with increased number of open DARs for Tregs on day 3. Thus, these effects on the chromatin landscape of Tregs are likely to contribute to the increased initial expansion to IL-2 when compared to Teff cells. The more rapid contraction is likely due in part to reduced mTORC1/pS6 dependent signaling leading to a chromatin landscape with reduced open DARs and lower energy metabolism.

Our findings have several interesting implications for ACT. The development of anti-cancer T cells used in ACT typically entails activation of polyclonal T cells with anti-CD3/CD28, engineering these activated T cells with CAR-T or cloned TCRs of desired specificity, and expansion with cytokines, where IL-2 has been most frequently used.[12] Since $CD4^+$ Teff cells have greater proliferative potential than Tregs, and $CD8^+$ Teff cells rapidly double after priming,[42] Tregs will be disadvantaged in the product for ACT. Nevertheless, Tregs remain a component of ACT used for tumor therapy and may sometimes be associated with limiting efficacy.[43–45] Determining more precisely the features that support contraction of Tregs may help to lower their presence for ACT of cancer. With respect to ACT of autoimmunity, bulk T cells are not used but rather Tregs must be purified before culture initiation. Our findings suggest that agonists that lead to increased PI3K/mTORC1 signaling and/or more energetic cells may improve Treg yields, although this might also run the risk of increasing the numbers of contaminating $CD4^+$ Teff cells. Indeed, rapamycin to inhibit mTORC1 is sometimes used in Treg expansion cultures to prevent the outgrowth of contaminating conventional $CD4^+$ T cells.[16–18]

Our study has interesting implications when interpreting our findings with respect to mechanisms that regulate tolerance and immunity. At homeostasis, human and mouse Tregs are the mostly highly proliferating lymphoid cells *in vivo*.[46–48] The basis for this high proliferative rate is not well understood, but it likely reflects in part integration of TCR, CD28, and IL-2R signaling during recognition of self-antigens. The sensing of more persistent IL-2R signaling by Tregs subsequently leads to chromatin remodeling that favors cessation of proliferation and contraction of Tregs. This potentially may represent a means by which the Treg TCR repertoire is not heavily skewed toward any one specificity. Induction of Blimp-1 in Tregs, which in part promotes Treg homeostasis, may represent one pathway to limit Tregs expansion to IL-2R signaling.[49,50] In addition, during an immune response IL-2 is likely more abundant and this along with the accompanying inflammatory response, which destabilizes Tregs[51,52] may facilitate expansion of Teff cells over Tregs. In a reciprocal manner, the heightened IL-2-dependent persistence of mTORC1/pS6 activation in Teff cells promotes metabolic processes to favor longer-term proliferation of Teff cells over Tregs.

This model is simplistic in that it only considers the potential outcomes of TCR, CD28, and IL-2R signaling as revealed by the *in vitro* behavior of human Treg and Teff cells. We contend that the distinct molecular programming of $CD4^+$ Treg and Teff cells revealed in our study contributes to regulating immune responses. However, Treg and Teff cells *in vivo* are also impacted by signaling from other co-stimulatory and co-inhibitory

(E) IPA predicted canonical pathways based on *Z* scores associated with the 1,921 unique DEGs (Figure 7D) induced by TCR/CD28/IL-2R in Tregs. Bubble plots of top canonical pathways as per *Z* score, which represents a measure of the predicted direction of the pathway activity. Each bubble represents a canonical pathway, and the bubble size is indicative of the number of genes that overlap the pathway. The bubble color represents *Z* scores as per the legend and color intensity is directly proportional to the *p* value, i.e., the more intense the color is, the more significant the result. Fisher's exact test ($p \leq 0.05$) was used to assess the canonical pathways correlated with the DEGs.

(F) IPA was used to overlay the predicted inhibited generic transcription pathway with DEGs from Tregs re-stimulated with either rhIL-2 or anti-CD3/CD28 beads and rhIL-2 for 72 h. Also see Figures S4 and S5; Table S10.

molecules as well as chemokines and other cytokines. The pathways associated with these types of molecules may either enhance or limit the capacities of Treg and Teff cells to distinctively respond to TCR, CD28, and IL-2R signaling. Consistent with our model, others and we have shown that IL-2R signaling favor $CD8^+$ anti-tumor T cells responses by reprogramming exhausted T cells even though Tregs also concurrently react to IL-2.[53–55] In contrast, low-dose IL-2 effectively expands Tregs, but not Teff cells, upon repeated application.[8,9] This response to low-dose IL-2 occurs in an environment where other pathways are likely engaged and may not solely be the outcome of persistent IL-2R signaling. Furthermore, low-dose IL-2 does not stimulate self-reactive Teff cells, and as such, avoids the potential of persistent IL-2R signaling to favor Teff cells. Overall, our data provide a framework to explore the molecular and genetic basis by which Treg and Teff cells respond to major signals required for the activation and expansion of these critical cells driving tolerance and immunity.

Limitations of the study

In this study, we compared the proliferative activity of Treg and Teff cells *in vitro* in response to TCR/CD28/IL-2R stimulation and investigated the underlying molecular basis of these responses. However, these analyses were performed with a small sample size, which limits the detection of more subtle factors and the study of confounding variables. In addition, all blood donors were males. Thus, our findings do not address whether there may be a sex difference related to the Treg and Teff cell expansion, gene expression, or chromatin remodeling. Our experiments were not designed to assess the impact of co-stimulatory and co-inhibitory molecules, chemokines, and other cytokines that likely impact the regulation of Treg and Teff cells *in vivo*. Additionally, we have only proposed potential mechanisms that may explain, for example, Treg contraction, the more persistent expansion of $CD4^+$ Teff cells, or the differences between Treg and $CD4^+$ Teff cells in response to re-stimulation. In the future, further mechanistic studies are necessary to define the specific genes driving these varied responses and to extrapolate our findings to enhance the generation of Treg and Teff cells for ACT for the treatment of cancer or autoimmune diseases.

RESOURCE AVAILABILITY

Lead contact

Further information and requests should be directed to the lead contact, Thomas R. Malek (tmalek@med.miami.edu).

Materials availability

This study did not generate unique materials.

Data and code availability

Raw sequencing reads reported in this paper have been deposited at the National Center for Biotechnology Information (https://www.ncbi.nlm.nih.gov). Accession codes: RNA-seq: Treg cells at 4 and 16 h: PRJNA873116; Teff cells at 4 and 16 h: PRJNA1171423; Treg/Teff at days 1–12: PRJNA1176666. ATAC-seq: Treg/Teff at days 1–12: PRJNA1176656. This article does not report original code. Other data will be made available upon reasonable request by the lead contact.

ACKNOWLEDGMENTS

The authors thank the Flow Cytometry and Oncogenomic Cores of the Sylvester Comprehensive Cancer Center at the University of Miami (supported by NIH P30CA240139). We also thank the sequencing core of the Hussman Institute for Human Genomics, University of Miami. This research was supported by funding to T.R.M. from Bristol Myers Squibb and the NIH (R01 AI131648). The graphical abstract and the workflow in Figure S1 were generated with BioRender (https://BioRender.com).

AUTHOR CONTRIBUTIONS

Conception and design, T.R.M., A.M., and A.Y.; acquisition of data, A.M and A.Y.; analysis and interpretation of data, A.M., A.Y., Z.G., Y.B., L.N., A.V.V., and T.R.M.; manuscript writing, A.M. and T.R.M.; all authors edited and approved the manuscript.

DECLARATION OF INTERESTS

This research has been supported in part by a collaboration and sponsored research agreement with Bristol Myers Squibb to T.R.M.

STAR★METHODS

Detailed methods are provided in the online version of this paper and include the following:

- KEY RESOURCES TABLE
- EXPERIMENTAL MODEL AND STUDY PARTICIPANT DETAILS
- METHOD DETAILS
  - Cell purification
  - Cell culture
  - Antibodies and flow cytometry
  - Phospho STAT5 (pSTAT5) and phospho S6 (pS6) *in vitro* assays
  - Metabolism assays (Seahorse)
  - RNA-seq libraries preparation
  - RNA-seq analysis
  - ATAC-seq libraries preparation
  - ATAC-seq analysis
  - Enrichment of differentially accessible regions (DARs)
  - Relationship between differentially expressed genes
- QUANTIFICATION AND STATISTICAL ANALYSIS

SUPPLEMENTAL INFORMATION

Supplemental information can be found online at https://doi.org/10.1016/j.isci.2025.112553.

Received: January 6, 2025
Revised: March 18, 2025
Accepted: April 25, 2025
Published: April 29, 2025

REFERENCES

1. Shouse, A.N., LaPorte, K.M., and Malek, T.R. (2024). Interleukin-2 signaling in the regulation of T cell biology in autoimmunity and cancer. Immunity *57*, 414–428. https://doi.org/10.1016/j.immuni.2024.02.001.
2. Lio, C.W.J., and Hsieh, C.S. (2008). A two-step process for thymic regulatory T cell development. Immunity *28*, 100–111. https://doi.org/10.1016/j.immuni.2007.11.021.
3. Burchill, M.A., Yang, J., Vang, K.B., Moon, J.J., Chu, H.H., Lio, C.W.J., Vegoe, A.L., Hsieh, C.S., Jenkins, M.K., and Farrar, M.A. (2008). Linked T cell receptor and cytokine signaling govern the development of the regulatory T cell repertoire. Immunity *28*, 112–121. https://doi.org/10.1016/j.immuni.2007.11.022.

4. Chinen, T., Kannan, A.K., Levine, A.G., Fan, X., Klein, U., Zheng, Y., Gasteiger, G., Feng, Y., Fontenot, J.D., and Rudensky, A.Y. (2016). An essential role for the IL-2 receptor in T(reg) cell function. Nat. Immunol. *17*, 1322–1333. https://doi.org/10.1038/ni.3540.

5. Tai, X., Indart, A., Rojano, M., Guo, J., Apenes, N., Kadakia, T., Craveiro, M., Alag, A., Etzensperger, R., Badr, M.E., et al. (2023). How autoreactive thymocytes differentiate into regulatory versus effector CD4$^+$ T cells after avoiding clonal deletion. Nat. Immunol. *24*, 637–651. https://doi.org/10.1038/s41590-023-01469-2.

6. Toomer, K.H., Lui, J.B., Altman, N.H., Ban, Y., Chen, X., and Malek, T.R. (2019). Essential and non-overlapping IL-2Rα-dependent processes for thymic development and peripheral homeostasis of regulatory T cells. Nat. Commun. *10*, 1037. https://doi.org/10.1038/s41467-019-08960-1.

7. Fan, M.Y., Low, J.S., Tanimine, N., Finn, K.K., Priyadharshini, B., Germana, S.K., Kaech, S.M., and Turka, L.A. (2018). Differential Roles of IL-2 Signaling in Developing versus Mature Tregs. Cell Rep. *25*, 1204–1213.e4. https://doi.org/10.1016/j.celrep.2018.10.002.

8. Sharabi, A., Tsokos, M.G., Ding, Y., Malek, T.R., Klatzmann, D., and Tsokos, G.C. (2018). Regulatory T cells in the treatment of disease. Nat. Rev. Drug Discov. *17*, 823–844. https://doi.org/10.1038/nrd.2018.148.

9. Hernandez, R., Põder, J., LaPorte, K.M., and Malek, T.R. (2022). Engineering IL-2 for immunotherapy of autoimmunity and cancer. Nat. Rev. Immunol. *22*, 614–628. https://doi.org/10.1038/s41577-022-00680-w.

10. Hombach, A.A., Kofler, D., Hombach, A., Rappl, G., and Abken, H. (2007). Effective proliferation of human regulatory T cells requires a strong costimulatory CD28 signal that cannot be substituted by IL-2. J. Immunol. *179*, 7924–7931. https://doi.org/10.4049/jimmunol.179.11.7924.

11. Putnam, A.L., Brusko, T.M., Lee, M.R., Liu, W., Szot, G.L., Ghosh, T., Atkinson, M.A., and Bluestone, J.A. (2009). Expansion of human regulatory T-cells from patients with type 1 diabetes. Diabetes *58*, 652–662. https://doi.org/10.2337/db08-1168.

12. Ayala Ceja, M., Khericha, M., Harris, C.M., Puig-Saus, C., and Chen, Y.Y. (2024). CAR-T cell manufacturing: Major process parameters and next-generation strategies. J. Exp. Med. *221*, e20230903. https://doi.org/10.1084/jem.20230903.

13. Melenhorst, J.J., Chen, G.M., Wang, M., Porter, D.L., Chen, C., Collins, M.A., Gao, P., Bandyopadhyay, S., Sun, H., Zhao, Z., et al. (2022). Decade-long leukaemia remissions with persistence of CD4(+) CAR T cells. Nature *602*, 503–509. https://doi.org/10.1038/s41586-021-04390-6.

14. Good, Z., Spiegel, J.Y., Sahaf, B., Malipatlolla, M.B., Ehlinger, Z.J., Kurra, S., Desai, M.H., Reynolds, W.D., Wong Lin, A., Vandris, P., et al. (2022). Post-infusion CAR T(Reg) cells identify patients resistant to CD19-CAR therapy. Nat. Med. *28*, 1860–1871. https://doi.org/10.1038/s41591-022-01960-7.

15. Haradhvala, N.J., Leick, M.B., Maurer, K., Gohil, S.H., Larson, R.C., Yao, N., Gallagher, K.M.E., Katsis, K., Frigault, M.J., Southard, J., et al. (2022). Distinct cellular dynamics associated with response to CAR-T therapy for refractory B cell lymphoma. Nat. Med. *28*, 1848–1859. https://doi.org/10.1038/s41591-022-01959-0.

16. Marshall, G.P., 2nd, Cserny, J., Perry, D.J., Yeh, W.I., Seay, H.R., Elsayed, A.G., Posgai, A.L., and Brusko, T.M. (2018). Clinical applications of regulatory T cells in adoptive cell therapies. Cell Gene Ther. Insights *4*, 405–429. https://doi.org/10.18609/cgti.2018.042.

17. McCallion, O., Bilici, M., Hester, J., and Issa, F. (2023). Regulatory T-cell therapy approaches. Clin. Exp. Immunol. *211*, 96–107. https://doi.org/10.1093/cei/uxac078.

18. Ferreira, L.M.R., Muller, Y.D., Bluestone, J.A., and Tang, Q. (2019). Next-generation regulatory T cell therapy. Nat. Rev. Drug Discov. *18*, 749–769. https://doi.org/10.1038/s41573-019-0041-4.

19. Li, M.O., and Rudensky, A.Y. (2016). T cell receptor signalling in the control of regulatory T cell differentiation and function. Nat. Rev. Immunol. *16*, 220–233. https://doi.org/10.1038/nri.2016.26.

20. Huynh, A., DuPage, M., Priyadharshini, B., Sage, P.T., Quiros, J., Borges, C.M., Townamchai, N., Gerriets, V.A., Rathmell, J.C., Sharpe, A.H., et al. (2015). Control of PI(3) kinase in Treg cells maintains homeostasis and lineage stability. Nat. Immunol. *16*, 188–196. https://doi.org/10.1038/ni.3077.

21. Walsh, P.T., Buckler, J.L., Zhang, J., Gelman, A.E., Dalton, N.M., Taylor, D.K., Bensinger, S.J., Hancock, W.W., and Turka, L.A. (2006). PTEN inhibits IL-2 receptor-mediated expansion of CD4$^+$ CD25$^+$ Tregs. J. Clin. Investig. *116*, 2521–2531. https://doi.org/10.1172/JCI28057.

22. Lam, A.J., Haque, M., Ward-Hartstonge, K.A., Uday, P., Wardell, C.M., Gillies, J.K., Speck, M., Mojibian, M., Klein Geltink, R.I., and Levings, M.K. (2022). PTEN is required for human Treg suppression of costimulation in vitro. Eur. J. Immunol. *52*, 1482–1497. https://doi.org/10.1002/eji.202249888.

23. Gennert, D.G., Lynn, R.C., Granja, J.M., Weber, E.W., Mumbach, M.R., Zhao, Y., Duren, Z., Sotillo, E., Greenleaf, W.J., Wong, W.H., et al. (2021). Dynamic chromatin regulatory landscape of human CAR T cell exhaustion. Proc. Natl. Acad. Sci. USA *118*, e2104758118. https://doi.org/10.1073/pnas.2104758118.

24. Hollbacher, B., Duhen, T., Motley, S., Klicznik, M.M., Gratz, I.K., and Campbell, D.J. (2020). Transcriptomic profiling of human effector and regulatory T cell subsets identifies predictive population signatures. Immunohorizons *4*, 585–596. https://doi.org/10.4049/immunohorizons.2000037.

25. Bhairavabhotla, R., Kim, Y.C., Glass, D.D., Escobar, T.M., Patel, M.C., Zahr, R., Nguyen, C.K., Kilaru, G.K., Muljo, S.A., and Shevach, E.M. (2016). Transcriptome profiling of human FoxP3$^+$ regulatory T cells. Hum. Immunol. *77*, 201–213. https://doi.org/10.1016/j.humimm.2015.12.004.

26. Reading, J.L., Roobrouck, V.D., Hull, C.M., Becker, P.D., Beyens, J., Valentin-Torres, A., Boardman, D., Lamperti, E.N., Stubblefield, S., Lombardi, G., et al. (2021). Augmented expansion of treg cells from healthy and autoimmune subjects via adult progenitor cell co-culture. Front. Immunol. *12*, 716606. https://doi.org/10.3389/fimmu.2021.716606.

27. Jarvis, L.B., Rainbow, D.B., Coppard, V., Howlett, S.K., Georgieva, Z., Davies, J.L., Mullay, H.K., Hester, J., Ashmore, T., Van Den Bosch, A., et al. (2021). Therapeutically expanded human regulatory T-cells are super-suppressive due to HIF1A induced expression of CD73. Commun. Biol. *4*, 1186. https://doi.org/10.1038/s42003-021-02721-x.

28. Boroughs, A.C., Larson, R.C., Marjanovic, N.D., Gosik, K., Castano, A.P., Porter, C.B.M., Lorrey, S.J., Ashenberg, O., Jerby, L., Hofree, M., et al. (2020). A distinct transcriptional program in human car T cells bearing the 4-1BB signaling domain revealed by scRNA-Seq. Mol. Ther. *28*, 2577–2592. https://doi.org/10.1016/j.ymthe.2020.07.023.

29. Langer, L.F., Ward, J.M., and Archer, T.K. (2019). Tumor suppressor SMARCB1 suppresses super-enhancers to govern hESC lineage determination. Elife *8*, e45672. https://doi.org/10.7554/eLife.45672.

30. Zaman, M.M.U., Masuda, K., Nyati, K.K., Dubey, P.K., Ripley, B., Wang, K., Chalise, J.P., Higa, M., Hanieh, H., and Kishimoto, T. (2016). Arid5a exacerbates IFN-gamma-mediated septic shock by stabilizing T-bet mRNA. Proc. Natl. Acad. Sci. USA *113*, 11543–11548. https://doi.org/10.1073/pnas.1613307113.

31. Jain, N., Zhao, Z., Koche, R.P., Antelope, C., Gozlan, Y., Montalbano, A., Brocks, D., Lopez, M., Dobrin, A., Shi, Y., et al. (2024). Disruption of SUV39H1-Mediated H3K9 methylation sustains Car T-cell function. Cancer Discov. *14*, 142–157. https://doi.org/10.1158/2159-8290.CD-22-1319.

32. Greenberg, M.V.C., and Bourc'his, D. (2019). The diverse roles of DNA methylation in mammalian development and disease. Nat. Rev. Mol. Cell Biol. *20*, 590–607. https://doi.org/10.1038/s41580-019-0159-6.

33. Shan, F., Cillo, A.R., Cardello, C., Yuan, D.Y., Kunning, S.R., Cui, J., Lampenfeld, C., Williams, A.M., McDonough, A.P., Pennathur, A., et al. (2023). Integrated BATF transcriptional network regulates suppressive intratumoral regulatory T cells. Sci. Immunol. *8*, eadf6717. https://doi.org/10.1126/sciimmunol.adf6717.

34. Itahashi, K., Irie, T., Yuda, J., Kumagai, S., Tanegashima, T., Lin, Y.T., Watanabe, S., Goto, Y., Suzuki, J., Aokage, K., et al. (2022). BATF epigenetically and transcriptionally controls the activation program of regulatory T cells in human tumors. Sci. Immunol. *7*, eabk0957. https://doi.org/10.1126/sciimmunol.abk0957.

35. He, Y.Y., Zhou, H.F., Chen, L., Wang, Y.T., Xie, W.L., Xu, Z.Z., Xiong, Y., Feng, Y.Q., Liu, G.Y., Li, X., et al. (2022). The Fra-1: Novel role in regulating extensive immune cell states and affecting inflammatory diseases. Front. Immunol. *13*, 954744. https://doi.org/10.3389/fimmu.2022.954744.

36. Shin, H.J., Lee, J.B., Park, S.H., Chang, J., and Lee, C.W. (2009). T-bet expression is regulated by EGR1-mediated signaling in activated T cells. Clin. Immunol. *131*, 385–394. https://doi.org/10.1016/j.clim.2009.02.009.

37. Schutt, S.D., Wu, Y., Kharel, A., Bastian, D., Choi, H.J., Hanief Sofi, M., Mealer, C., McDaniel Mims, B., Nguyen, H., Liu, C., et al. (2022). The druggable transcription factor Fli-1 regulates T cell immunity and tolerance in graft-versus-host disease. J. Clin. Investig. *132*, e143950. https://doi.org/10.1172/JCI143950.

38. Newton, R., Priyadharshini, B., and Turka, L.A. (2016). Immunometabolism of regulatory T cells. Nat. Immunol. *17*, 618–625. https://doi.org/10.1038/ni.3466.

39. Battaglia, M., Stabilini, A., Migliavacca, B., Horejs-Hoeck, J., Kaupper, T., and Roncarolo, M.G. (2006). Rapamycin promotes expansion of functional $CD4^+CD25^+FOXP3$+ regulatory T cells of both healthy subjects and type 1 diabetic patients. J. Immunol. *177*, 8338–8347. https://doi.org/10.4049/jimmunol.177.12.8338.

40. Strauss, L., Whiteside, T.L., Knights, A., Bergmann, C., Knuth, A., and Zippelius, A. (2007). Selective survival of naturally occurring human $CD4^+$ $CD25^+Foxp3^+$ regulatory T cells cultured with rapamycin. J. Immunol. *178*, 320–329. https://doi.org/10.4049/jimmunol.178.1.320.

41. Chi, H. (2012). Regulation and function of mTOR signalling in T cell fate decisions. Nat. Rev. Immunol. *12*, 325–338. https://doi.org/10.1038/nri3198.

42. De Boer, R.J., Homann, D., and Perelson, A.S. (2003). Different dynamics of CD4+ and CD8+ T cell responses during and after acute lymphocytic choriomeningitis virus infection. J. Immunol. *171*, 3928–3935. https://doi.org/10.4049/jimmunol.171.8.3928.

43. Sakaguchi, S., Yamaguchi, T., Nomura, T., and Ono, M. (2008). Regulatory T cells and immune tolerance. Cell *133*, 775–787. https://doi.org/10.1016/j.cell.2008.05.009.

44. Tanaka, A., and Sakaguchi, S. (2017). Regulatory T cells in cancer immunotherapy. Cell Res. *27*, 109–118. https://doi.org/10.1038/cr.2016.151.

45. Colombo, M.P., and Piconese, S. (2007). Regulatory-T-cell inhibition versus depletion: the right choice in cancer immunotherapy. Nat. Rev. Cancer *7*, 880–887. https://doi.org/10.1038/nrc2250.

46. Attridge, K., and Walker, L.S.K. (2014). Homeostasis and function of regulatory T cells (Tregs) in vivo: lessons from TCR-transgenic Tregs. Immunol. Rev. *259*, 23–39. https://doi.org/10.1111/imr.12165.

47. Malek, T.R., Yu, A., Vincek, V., Scibelli, P., and Kong, L. (2002). CD4 regulatory T cells prevent lethal autoimmunity in IL-2Rβ-deficient mice. Implications for the nonredundant function of IL-2. Immunity *17*, 167–178. https://doi.org/10.1016/s1074-7613(02)00367-9.

48. Vukmanovic-Stejic, M., Zhang, Y., Cook, J.E., Fletcher, J.M., McQuaid, A., Masters, J.E., Rustin, M.H.A., Taams, L.S., Beverley, P.C.L., Macallan, D. C., and Akbar, A.N. (2006). Human CD4+ CD25hi Foxp3+ regulatory T cells are derived by rapid turnover of memory populations in vivo. J. Clin. Investig. *116*, 2423–2433. https://doi.org/10.1172/JCI28941.

49. Cretney, E., Leung, P.S., Trezise, S., Newman, D.M., Rankin, L.C., Teh, C. E., Putoczki, T.L., Gray, D.H., Belz, G.T., Mielke, L.A., et al. (2018). Characterization of Blimp-1 function in effector regulatory T cells. J. Autoimmun. *91*, 73–82. https://doi.org/10.1016/j.jaut.2018.04.003.

50. Bankoti, R., Ogawa, C., Nguyen, T., Emadi, L., Couse, M., Salehi, S., Fan, X., Dhall, D., Wang, Y., Brown, J., et al. (2017). Differential regulation of effector and regulatory T cell function by Blimp1. Sci. Rep. *7*, 12078. https://doi.org/10.1038/s41598-017-12171-3.

51. Oldenhove, G., Bouladoux, N., Wohlfert, E.A., Hall, J.A., Chou, D., Dos Santos, L., O'Brien, S., Blank, R., Lamb, E., Natarajan, S., et al. (2009). Decrease of $Foxp3^+$ Treg cell number and acquisition of effector cell phenotype during lethal infection. Immunity *31*, 772–786. https://doi.org/10.1016/j.immuni.2009.10.001.

52. Kastner, L., Dwyer, D., and Qin, F.X.F. (2010). Synergistic effect of IL-6 and IL-4 in driving fate revision of natural $Foxp3^+$ regulatory T cells. J. Immunol. *185*, 5778–5786. https://doi.org/10.4049/jimmunol.0901948.

53. LaPorte, K.M., Hernandez, R., Santos Savio, A., and Malek, T.R. (2023). Robust IL-2-dependent antitumor immunotherapy requires targeting the high-affinity IL-2R on tumor-specific $CD8^+$ T cells. J. Immunother. Cancer *11*, e006611. https://doi.org/10.1136/jitc-2022-006611.

54. West, E.E., Jin, H.T., Rasheed, A.U., Penaloza-Macmaster, P., Ha, S.J., Tan, W.G., Youngblood, B., Freeman, G.J., Smith, K.A., and Ahmed, R. (2013). PD-L1 blockade synergizes with IL-2 therapy in reinvigorating exhausted T cells. J. Clin. Investig. *123*, 2604–2615. https://doi.org/10.1172/JCI67008.

55. Codarri Deak, L., Nicolini, V., Hashimoto, M., Karagianni, M., Schwalie, P. C., Lauener, L., Varypataki, E.M., Richard, M., Bommer, E., Sam, J., et al. (2022). PD-1-cis IL-2R agonism yields better effectors from stem-like $CD8^+$ T cells. Nature *610*, 161–172. https://doi.org/10.1038/s41586-022-05192-0.

56. Dobin, A., Davis, C.A., Schlesinger, F., Drenkow, J., Zaleski, C., Jha, S., Batut, P., Chaisson, M., and Gingeras, T.R. (2013). STAR: ultrafast universal RNA-seq aligner. Bioinformatics *29*, 15–21. https://doi.org/10.1093/bioinformatics/bts635.

57. Liao, Y., Smyth, G.K., and Shi, W. (2014). featureCounts: an efficient general purpose program for assigning sequence reads to genomic features. Bioinformatics *30*, 923–930. https://doi.org/10.1093/bioinformatics/btt656.

58. Love, M.I., Huber, W., and Anders, S. (2014). Moderated estimation of fold change and dispersion for RNA-seq data with DESeq2. Genome Biol. *15*, 550. https://doi.org/10.1186/s13059-014-0550-8.

59. Trapnell, C., Roberts, A., Goff, L., Pertea, G., Kim, D., Kelley, D.R., Pimentel, H., Salzberg, S.L., Rinn, J.L., and Pachter, L. (2012). Differential gene and transcript expression analysis of RNA-seq experiments with TopHat and Cufflinks. Nat. Protoc. *7*, 562–578. https://doi.org/10.1038/nprot.2012.016.

60. Anders, S., Pyl, P.T., and Huber, W. (2015). HTSeq–a Python framework to work with high-throughput sequencing data. Bioinformatics *31*, 166–169. https://doi.org/10.1093/bioinformatics/btu638.

61. Gaspar, J.M. (2018). NGmerge: merging paired-end reads via novel empirically-derived models of sequencing errors. BMC Bioinf. *19*, 536. https://doi.org/10.1186/s12859-018-2579-2.

62. Langmead, B., and Salzberg, S.L. (2012). Fast gapped-read alignment with Bowtie 2. Nat. Methods *9*, 357–359. https://doi.org/10.1038/nmeth.1923.

63. Ramirez, F., Ryan, D.P., Gruning, B., Bhardwaj, V., Kilpert, F., Richter, A. S., Heyne, S., Dundar, F., and Manke, T. (2016). deepTools2: a next generation web server for deep-sequencing data analysis. Nucleic Acids Res. *44*, W160–W165. https://doi.org/10.1093/nar/gkw257.

64. Orchard, P., Kyono, Y., Hensley, J., Kitzman, J.O., and Parker, S.C.J. (2020). Quantification, dynamic visualization, and validation of bias in ATAC-Seq data with ataqv. Cell Syst. *10*, 298–306.e4. https://doi.org/10.1016/j.cels.2020.02.009.

65. Wu, M., and Gu, L.. TCseq: Time course sequencing data analysis. https://bioconductor.org/packages/release/bioc/html/TCseq.html.

66. Robinson, J.T., Thorvaldsdóttir, H., Winckler, W., Guttman, M., Lander, E. S., Getz, G., and Mesirov, J.P. (2011). Integrative genomics viewer. Nat. Biotechnol. *29*, 24–26. https://doi.org/10.1038/nbt.1754.

67. Nagraj, V.P., Magee, N.E., and Sheffield, N.C. (2018). LOLAweb: a containerized web server for interactive genomic locus overlap

enrichment analysis. Nucleic Acids Res. *46*, W194–W199. https://doi.org/10.1093/nar/gky464.

68. Chen, E.Y., Tan, C.M., Kou, Y., Duan, Q., Wang, Z., Meirelles, G.V., Clark, N.R., and Ma'ayan, A. (2013). Enrichr: interactive and collaborative HTML5 gene list enrichment analysis tool. BMC Bioinf. *14*, 128. https://doi.org/10.1186/1471-2105-14-128.
69. Krämer, A., Green, J., Pollard, J., Jr., and Tugendreich, S. (2014). Causal analysis approaches in Ingenuity Pathway Analysis. Bioinformatics *30*, 523–530. https://doi.org/10.1093/bioinformatics/btt703.
70. Yu, A., Snowhite, I., Vendrame, F., Rosenzwajg, M., Klatzmann, D., Pugliese, A., and Malek, T.R. (2015). Selective IL-2 responsiveness of regulatory T cells through multiple intrinsic mechanisms supports the use of low--dose IL-2 therapy in type 1 diabetes. Diabetes *64*, 2172–2183. https://doi.org/10.2337/db14-1322.
71. Mookerjee, S.A., Gerencser, A.A., Nicholls, D.G., and Brand, M.D. (2018). Quantifying intracellular rates of glycolytic and oxidative ATP production and consumption using extracellular flux measurements. J. Biol. Chem. *293*, 12649–12652. https://doi.org/10.1074/jbc.AAC118.004855.
72. Rau, A., Gallopin, M., Celeux, G., and Jaffrézic, F. (2013). Data-based filtering for replicated high-throughput transcriptome sequencing experiments. Bioinformatics *29*, 2146–2152. https://doi.org/10.1093/bioinformatics/btt350.
73. Anders, S., McCarthy, D.J., Chen, Y., Okoniewski, M., Smyth, G.K., Huber, W., and Robinson, M.D. (2013). Count-based differential expression analysis of RNA sequencing data using R and Bioconductor. Nat. Protoc. *8*, 1765–1786. https://doi.org/10.1038/nprot.2013.099.
74. Yu, G., Wang, L.G., Han, Y., and He, Q.Y. (2012). clusterProfiler: an R package for comparing biological themes among gene clusters. OMICS *16*, 284–287. https://doi.org/10.1089/omi.2011.0118.
75. Liberzon, A., Birger, C., Thorvaldsdóttir, H., Ghandi, M., Mesirov, J.P., and Tamayo, P. (2015). The Molecular Signatures Database (MSigDB) hallmark gene set collection. Cell Syst. *1*, 417–425. https://doi.org/10.1016/j.cels.2015.12.004.
76. Corces, M.R., Trevino, A.E., Hamilton, E.G., Greenside, P.G., Sinnott-Armstrong, N.A., Vesuna, S., Satpathy, A.T., Rubin, A.J., Montine, K.S., Wu, B., et al. (2017). An improved ATAC-seq protocol reduces background and enables interrogation of frozen tissues. Nat. Methods *14*, 959–962. https://doi.org/10.1038/nmeth.4396.
77. Heinz, S., Benner, C., Spann, N., Bertolino, E., Lin, Y.C., Laslo, P., Cheng, J.X., Murre, C., Singh, H., and Glass, C.K. (2010). Simple combinations of lineage-determining transcription factors prime cis-regulatory elements required for macrophage and B cell identities. Mol. Cell *38*, 576–589. https://doi.org/10.1016/j.molcel.2010.05.004.
78. Ross-Innes, C.S., Stark, R., Teschendorff, A.E., Holmes, K.A., Ali, H.R., Dunning, M.J., Brown, G.D., Gojis, O., Ellis, I.O., Green, A.R., et al. (2012). Differential oestrogen receptor binding is associated with clinical outcome in breast cancer. Nature *481*, 389–393. https://doi.org/10.1038/nature10730.
79. Kuleshov, M.V., Jones, M.R., Rouillard, A.D., Fernandez, N.F., Duan, Q., Wang, Z., Koplev, S., Jenkins, S.L., Jagodnik, K.M., Lachmann, A., et al. (2016). Enrichr: a comprehensive gene set enrichment analysis web server 2016 update. Nucleic Acids Res. *44*, W90–W97. https://doi.org/10.1093/nar/gkw377.
80. Xie, Z., Bailey, A., Kuleshov, M.V., Clarke, D.J.B., Evangelista, J.E., Jenkins, S.L., Lachmann, A., Wojciechowicz, M.L., Kropiwnicki, E., Jagodnik, K.M., et al. (2021). Gene set knowledge discovery with Enrichr. Curr. Protoc. *1*, e90. https://doi.org/10.1002/cpz1.90.
81. Oliveros, J.C. (2007). Venny. An interactive tool for comparing lists with Venn's diagrams. https://bioinfogp.cnb.csic.es/tools/venny/index.html.

STAR★METHODS

KEY RESOURCES TABLE

REAGENT or RESOURCE	SOURCE	IDENTIFIER
Antibodies		
BV421 Mouse Anti-Human CD25	BD Biosciences	M-A251; Cat#562442; RRID: AB_11154578
Alexa Fluor 647 Mouse anti-Human CD127	BD Biosciences	HIL-7R-M21; Cat#558598; RRID: AB_647113
Alexa Fluor 700 Mouse Anti-Human CD45RA	BD Biosciences	HI100; Cat#560673; RRID: AB_1727496
FITC Mouse Anti-Human CD4	BD Biosciences	RPA-T4; Cat#555346; RRID: AB_395751
PE Mouse anti-Human FoxP3	BD Biosciences	259D/C7; Cat#560046; RRID: AB_1645508
Alexa Fluor 700 Mouse anti-Ki-67	BD Biosciences	B56; Cat#561277; RRID: AB_10611571
Alexa Fluor 488 Anti-Stat5 (pY694)	BD Biosciences	47; Cat# 612598; RRID: AB_399881
Alexa Fluor 488 phosphoS6 (Ser235/236)	Cell Signaling Technology	2F9; Cat# 4854S; RRID: AB_390782
Purified anti-human CD3 Antibody	Biolegend	OKT3; Cat#317301; AB_571926
Purified anti-human CD28 Antibody	Biolegend	28.2; Cat#302901; RRID: AB_314303
Biological samples		
Human peripheral blood samples	Continental blood bank, Miami	https://www.continentalbloodbank.com/
Chemicals, peptides, and recombinant proteins		
Fixable Viability Dye eFluor™ 455UV	ThermoFisher Scientific	Cat# 00-5523-00
Human IL-2	ThermoFisher Scientific	Cat#200-02
Critical commercial assays		
Foxp3/Transcription Factor Staining Buffer Set	ThermoFisher Scientific	Cat# 65-0868-18
Seahorse XF Cell Mito Stress Test Kit	Agilent	103010-100
Nextera DNA Library Prep kit	Illumina	15028212
Deposited data		
RNAseq, Treg; 4-16 hr	This paper	NCBI: PRJNA873116
RNAseq, Teff; 4-16 hr	This paper	NCBI: PRJNA1171423
RNAseq, Days 1-12	This paper	NCBI: PRJNA1176666
ATACseq, Days 1-12	This paper	NCBI: PRJNA1176656
Software and algorithms		
STAR aligner	Dobin et al.[56]	http://code.google.com/p/rna-star
featureCounts	Liao et al.[57]	https://subread.sourceforge.net
DESeq2	Love et al.[58]	http://www.bioconductor.org/packages/release/bioc/html/DESeq2.html
TopHat2	Trapnell et al.[59]	http://tophat.cbcb.umd.edu
Cufflinks	Trapnell et al.[59]	http://cufflinks.cbcb.umd.edu
HTseq-count	Anders et al.[60]	http://www-huber.embl.de/HTSeq
NGmerge	Gaspar[61]	https://github.com/harvardinformatics/NGmerge
Bowtie2	Langmead and Salzberg[62]	http://bowtie-bio.sourceforge.net/bowtie2/index.shtml
deepTools2	Ramirez et al.[63]	http://deeptools.ie-freiburg.mpg.de
ATAQV	Orchard et al.[64]	https://github.com/ParkerLab/ataqv
TCseq	Wu and Gu[65]	https://bioconductor.org/packages/release/bioc/html/TCseq.html
Integrative genomics viewer	Robinson et al.[66]	https://igv.org
Locus amplification analysis software	Nagraj et al.[67]	http://github.com/databio/LOLAweb
Enrich	Chen et al.[68]	https://maayanlab.cloud/Enrichr/
Morpheus		https://software.broadinstitute.org/morpheus/
Ingenuity Pathway Analysis	Kramer et al.[69]	https://www.qiagenbioinformatics.com/products/ingenuity-pathway-analysis/

EXPERIMENTAL MODEL AND STUDY PARTICIPANT DETAILS

De-identified peripheral blood samples were purchased from Continental Blood Bank, (Miami, FL). Donors were healthy adult males between 19-45 years of age (31.2 ± 9.1; mean ± SD). Seven donors were Black (4), Hispanic Black (2), and Hispanic Caucasian (1). Treg and Teff cells were isolated from each donor, and these cells were expanded with anti-CD3/CD28 beads and IL-2, as indicated. The unstimulated cells from each donor served as the control. This study is non-human subjects research as reviewed by the IRB at the University of Miami.

METHOD DETAILS

Cell purification

Heparinized leukocyte unit was diluted in PBS (1:1 final ratio), layered on Ficoll-Paque Plus (GE Healthcare, Little Chalfont, U.K.) and centrifuged at 400g for 30 min at room temperature without braking. PBMCs from the interphase cells were collected and washed once with PBS. Human $CD4^+$ T cells were enriched from PBMCs by negative selection with the MACS $CD4^+$ T Cell Isolation Kit (Miltenyi Biotec, Auburn, CA).

The $CD4^+$ T cells were stained by FITC-αCD4, BV421-αCD25, APC-αCD127, and Alexa Flour700-αCD45RA and sorted by using a BD FACS Aria-II sorter. Purity of sorted cells was further evaluated by FOXP3 expression after counter staining with PE-αFOXP3. Treg cells were obtained by sorting $CD4^+$ $CD25^{hi}$ $CD127^{lo}$ cells ($\geq$96%$^+$ post sort, typically >90% $FOXP3^+$). T effector (Teff) cells were obtained by sorting $CD4^+$ $CD127^{hi}$ $CD25^{lo/-}$ cells that were also $CD45RA^-$ ($\geq$97%+ post sort, typically 1-2% $FOXP3^+$).

Cell culture

FACS-sorted Treg or T_{EM} cells (7×10^5/well) were cultured in 24 well flat bottom plates with anti-CD3/CD28 (Dynabeads, ThermoFisher Scientific) and human IL-2 (500 unit/ml, Novartis) in 1 ml of OpTmizer CTS™ T cell expansion medium (designated as SFM) (Life Technologies, Grand Islands, NY). The ratio of beads to cells was 4:1. 24 hr later an additional 1 ml of SFM medium containing IL-2 (500 U/ml) was added to the cultures. On day 3 the cells were harvested and replated at 1 x10^5/well in in 2 ml of SFM medium containing IL-2 (500U/m). On days 6 and 9 cells were harvested and replated at 3×10^5/well in 2 ml of medium containing IL-2 (500 U/ml). On day 9 some cultures were restimulated with anti-CD3/CD28 beads (1:1 ratio, cells to beads) and IL-2 (500 U/ml).

Antibodies and flow cytometry

The following monoclonal anti-human antibodies (with the clone names in parenthesis) were obtained from BD Biosciences (San Jose, CA), Biolegend (San Diego, CA), or Cell Signaling (Danvers, MA): FITC/-αCD4 (RPA-T4), APC-αCD127 (A019D5), Alexa Fluor 700-αCD45RA (HI100), BV421-αCD25 (M-A251), PE-αFOXP3 (259D), Alexa Fluor 700-αKi67 (B56), Alexa Fluor 488-αphosphorylated STAT5 (47), and Alexa Fluor 488-αpS6 (2F9). Fixable Viability Dye eFluor 455UV were purchased from ThermoFisher Scientific (Vilnius, LT).

Cell-surface staining was performed with antibodies in FACS buffer (HBSS, 0.2% BSA, 0.1% sodium azide) for 15 min at 4°C. Intracellular staining for FOXP3/KI67 was performed after fixing and permeabilizing using FOXP3/Transcription Factor Staining Buffer Set (eBioscience) according to the manufacturer's instructions. For pSTAT5 and pS6 staining, cells were fixed with paraformaldehyde and permeabilized using ice-cold 100% methanol (see below). FACS analysis was performed using a BD LSRFortessa (Beckman Coulter) flow cytometer, where typically 100,000 events were collected. Data was analyzed using BD FACSDiva 8.0.1 or FlowJo v10.7.1 software, where viable cells were gated based on forward versus side light scatter profiles and doublets were excluded based on forward light scatter area versus scatter width.

Phospho STAT5 (pSTAT5) and phospho S6 (pS6) *in vitro* assays

Treg and Teff cells were washed 3 times with PBS and cultured in SFM (1-5 x 10^5/ml) for 4 hr in 5% CO_2 at 37°C. hIL-2 (500 U/mL) was then added for 15 min at 37°C. The pSTAT5 staining was performed as previously described.[70] For pS6 analysis, Treg and Teff cells were stimulated with plate bound anti-CD3 (OKT3, Biolegend), soluble anti-CD28 (CD28.2, Biolegend) for 3 hr at 37°C in 5% CO_2. After stimulation, cells were fixed, permeabilized, and stained for specific antibodies.

Metabolism assays (Seahorse)

Treg and Teff cells were cultured as described above. At the indicated times, cells were harvested and plated at 2×10^5 cells/well using Cell-Tak (Corning). The oxygen consumption rates (OCR) and extracellular acidification rates (ECAR) were measured under basal conditions and in response to 2 μM of the mitochondrial inhibitor oligomycin, 8 μM of the mitochondrial uncoupler FCCP, and 2 μM of the respiratory chain inhibitors antimycin A/rotenone using the Agilent Seahorse XFp Extracellular Flux Analyzer (Agilent).[71] Data was analyzed with the software Wave (Agilent, version 2.6.0.31).

RNA-seq libraries preparation

Treg or Teff cells (4-6 biological replicates) were pelleted after indicated times and resuspended in TRIzol (Thermo Fisher Scientific). The RNA was isolated using the RNeasy Micro Kit (Qiagen) according to the manufacturer's instructions. Quality control analysis,

library generation, and RNA-seq were carried out by the Oncogenomics Core Facility at the University of Miami. Quality control analysis of RNA samples was performed using the Bioanalyzer 2100 platform (Agilent Technologies). Libraries were prepared using the KAPA's RNA Hyperprep with RiboErase HMR protocol at the Oncogenomics Core at the University of Miami. Libraries from early induction experiment (4-16 hr) samples were sequenced with 25 million single-end 100 base reads/sample (per lane) using the Illumina HiSeq SE1000 at the sequencing core of the Center for Genome Technology, Hussman Institute for Human Genomics, University of Miami. Libraries from the longitudinal study (Days 1-12) were sequenced 40 million paired-end 75 base reads/sample (per lane) using the Illumina Novaseq XP at the Oncogenomics core at the University of Miami.

RNA-seq analysis

For the experiments at 4-16 hr, reads from the RNA-seq were mapped to the Homo sapiens (human) genome GRCh38 using STAR aligner (v2.5.0).[56] Raw counts were generated based on the Ensembl genes (GENCODE v27) with featureCounts (v1.5.0).[57] Differentially expressed genes (DEGs) were identified using DESeq2[58] and determined using a threshold of FDR $\leq$0.01.

For the experiments at 1-12 days, 50-70 bp reads were quality controlled (FastQC), aligned to human reference genome build hg38 (Tophat2),[59] assembled into transcripts (Cufflinks)[59] and gene-level counts compiled with htseq-count.[60] To minimize normalization artifacts, transcripts failing to reach an empirically defined count threshold were purged (htsfilter).[72] Next, filtered counts were normalized and pairwise comparisons performed to call ((DEG) edgeR; called by quasi-likelihood F testing).[73] DEG call denotes >2 fold pairwise change, and Benjamini-Hochberg (BH) adjusted p value <0.05. Transcripts Per Million (TPM) were also compiled (edgeR). Genes failing to reach 2 TPM in any condition were purged, as were micro-RNAs, sno-RNAs and sca-RNAs. An offset value of 1 was then added to all remaining entries. TPM+1 was used as input for Euclidian clustering (hclust, pheatmap) and principal component analysis (prcomp). For pathway analysis, input genesets were defined based on DEG (RNA-seq) and/or DAR (ATAC-seq), then hypergeometric testing was performed against the Molecular Signature (MSigDB) database (clusterprofileR).[74,75]

ATAC-seq libraries preparation

The Assay for Transposase-Accessible Chromatin using Sequencing (ATAC-seq) was performed as previously described.[76] 50,000 unfixed nuclei derived from Treg or Teff (4 biological replicates) were tagged using the Tn5 transposase (Nextera DNA sample prep kit; Illumina) for 30 min at 37°C. Libraries were generated using the Ad1_noMX and Ad2.1-24 barcoded primers and amplified for 10-12 cycles. Resulting libraries fragments were purified using a DNA Clean & Concentrator-5 kit (Zymo Research). Size-selection was performed using the Agencourt AMPure XP PCR purification system (Beckman Coulter) to remove large fragments >1 kb and primers to maintain high library complexity. Quality control analysis of libraries using the Agilent Bioanalyzer High-Sensitivity DNA kit and sequences with a 75 bp pair-end run to a minimum depth of 40 million reads per sample using the Illumina Novaseq XP sequencer (150 cycle; 400 M flow cell) were performed at the Oncogenomics Core of the University of Miami.

ATAC-seq analysis

Short, 50-70 bp reads were quality controlled (FastQC), trimmed to remove adapters (NGmerge),[61] aligned to human reference genome build hg38 (Bowtie2),[62] sorted (Samtools), and 'shifted' + 4 bp and − 4 bp on positive and negative strands, respectively, to account for 8-bp DNA repair artifacts created by Tn5 transposase nicking (deepTools 2 AlignmentSieve).[63] Next, peaks were called (Genrich), quality controlled (atacqv),[64] annotated (Homer AnnotatePeaks)[77] and pairwise comparisons performed to identify Differentially Accessible Regions (DARs called will Diffbind).[78] For downstream analysis, peaks and DAR are assigned to genes if they are located +/- 10kb from transcriptional start site (TSS) or within the gene body (introns/exons). TCseq was used for time course analysis of both RNA-seq and ATAC-seq.[65] Genome browser files were generated with Homer BedGraphToBigWig and rendered using Integrated Genome Viewer (Broad Institute).[66]

Enrichment of differentially accessible regions (DARs)

To infer genomic regions present in clusters derived from the TCseq analysis of DARs regions (query) in Treg and Teff cells that overlap with each region set in a compendium of publicly available region sets (database), Locus amplification analysis software (LOLA) as well as its composited database (version 1.12.0) was used.[67] Only peaks sets with membership scores >0.8 were analyzed. The LOLA analysis included databases from ENCODE and NIH Human Epigenomics projects.

Relationship between differentially expressed genes

For gene ontology analysis, input genes were tested against MSigDB 2020 Hallmark database using web-based tool Enrich.[68,79,80] DEGs were grouped and heat maps were constructed by hierarchical clustering of DEGs (rows) and indicated treatment conditions (columns). Hierarchical clustering (one minus the Pearson correlation, k-means partition tool) was performed using the matrix visualization and analysis tool Morpheus (https://software.broadinstitute.org/morpheus).

DEGs from RNA-seq were uploaded into Qiagen's Ingenuity Pathway Analysis IPA software[69] (https://www.qiagenbioinformatics.com/products/ingenuity-pathway-analysis/) for core analysis with cutoffs set at fold changes $\geq$ log [1] and FDR $\leq$0.01 to identify significantly DEGs. A heatmap was used to demonstrate differences in the expression of transcription factors and canonical pathways between Treg and Teff at day 9. On day 12, a subset of 1921 unique differentially expressed genes (DEGs) (fold changes $\geq$ log[1] and FDR $\leq$0.01) identified in Tregs stimulated on day 9 with anti-CD3/CD28 + hIL-2, but not with hIL-2 alone, was overlaid with the

generic transcription factor network in IPA. Network map analysis was used to demonstrate the differences in the expression patterns of these DEGs between the two conditions. The web tool Venny 2.1 was used to show relations between differentially expressed genes.[81]

QUANTIFICATION AND STATISTICAL ANALYSIS

Statistical analysis was performed using GraphPad Prism software (version 10.2.3). Data are shown as mean ± SEM. Two-tailed paired Student's tests were used for comparing two groups (Figures 6C and 6D). The two-way ANOVA comparison test was used to calculate statistical significance among groups. Statistical details and significance levels can be found in figure legends.